

Chapter 10

Spin-Flip TDDFT for Photochemistry

John M. Herbert and Aniket Mandal

*Department of Chemistry and Biochemistry, The Ohio State University,
Columbus, Ohio USA*
herbert@chemistry.ohio-state.edu

10.1 Computational Photochemistry

10.1.1 Conical Intersections

Conical intersections (CXs) play a central role in photophysics and photochemistry [74, 97], serving as the “funnels” for nonadiabatic dynamics between coupled potential energy surfaces representing different electronic states [1, 71, 125]. For the special case of two coupled electronic states, the CX is really a “conical seam” of dimension $N_{\text{int}} - 2$ where N_{int} is the number of internal (vibrational) degrees of freedom. Within this $(N_{\text{int}} - 2)$ -dimensional subspace the two states in question are degenerate, and when plotted in two dimensions this seam collapses to a point and the topology is that of a double cone, hence “CX.” For points within the seam space, even an infinitesimal displacement outside of this space will lift the degeneracy, and this two-dimensional “branching space” is spanned

Time-Dependent Density Functional Theory: Nonadiabatic Molecular Dynamics

Edited by Chaoyuan Zhu

Copyright © 2023 Jenny Stanford Publishing Pte. Ltd.

ISBN 978-981-4968-42-3 (Hardcover), 978-1-003-31921-4 (eBook)

www.jennystanford.com

by a pair of nonorthogonal vectors that are usually labeled \mathbf{g} and \mathbf{h} . For a two-state intersection between Born–Oppenheimer electronic potential energy surfaces $E_J(\mathbf{R})$ and $E_K(\mathbf{R})$, these branching-plane vectors consist of the *gradient-difference vector*,

$$\mathbf{g}_{JK}(\mathbf{R}) = \hat{\nabla}_{\mathbf{R}} [E_J(\mathbf{R}) - E_K(\mathbf{R})], \quad (10.1)$$

which is simply the difference in slopes between the two surfaces, and the *nonadiabatic coupling vector*,

$$\mathbf{h}_{JK}(\mathbf{R}) = \langle \Psi_J(\mathbf{R}) | \hat{\nabla}_{\mathbf{R}} \hat{H}(\mathbf{R}) | \Psi_K(\mathbf{R}) \rangle. \quad (10.2)$$

In both equations, \mathbf{R} represents the nuclear coordinates that define the potential energy surface and $\hat{\nabla}_{\mathbf{R}}$ indicates the vector-valued operator consisting of derivatives with respect to these coordinates. The quantities $|\Psi_J(\mathbf{R})\rangle$ and $|\Psi_K(\mathbf{R})\rangle$ are the Born–Oppenheimer electronic wavefunctions for electronic states J and K , defined by

$$\hat{H}|\Psi_K\rangle = E_K|\Psi_K\rangle \quad (10.3)$$

but written as $|\Psi_K(\mathbf{R})\rangle$ in Eq. (10.2) to remind the reader that the Born–Oppenheimer wavefunctions depend upon the geometry \mathbf{R} at which Eq. (10.3) is solved.

As a simple example, two different CXs for the ethylene molecule are plotted in Fig. 10.1. As indicated by the molecular structures, these photochemical funnels are often associated with bond breaking and access very different geometries as compared to those sampled in ground-state dynamics. To access the “twisted-pyramidalized” CX in Fig. 10.1a, $\pi \rightarrow \pi^*$ excitation from the ground state leads to dissolution of the C=C double bond followed by rotation around the intact σ bond. In the “ethylidene” CX of Fig. 10.1b, a hydrogen atom has transferred from one carbon atom to the other.

The dimension of the branching-plane vectors \mathbf{g}_{JK} and \mathbf{h}_{JK} is that of \mathbf{R} . For a single nuclear coordinate x , a simplified notation is

$$g_{JK}^{[x]} = \frac{\partial E_J(\mathbf{R})}{\partial x} - \frac{\partial E_K(\mathbf{R})}{\partial x} \quad (10.4a)$$

$$h_{JK}^{[x]} = \langle \Psi_J(\mathbf{R}) | (\partial \hat{H} / \partial x) | \Psi_K(\mathbf{R}) \rangle. \quad (10.4b)$$

The nonadiabatic coupling vector \mathbf{h}_{JK} is related to the (first-order) derivative coupling vector, defined as

$$\mathbf{d}_{JK}(\mathbf{R}) = \langle \Psi_J(\mathbf{R}) | \hat{\nabla}_{\mathbf{R}} \Psi_K(\mathbf{R}) \rangle, \quad (10.5)$$

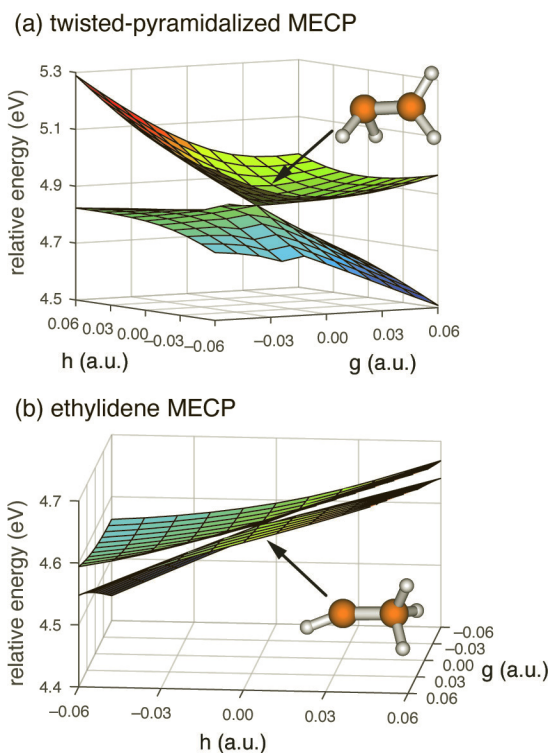


Figure 10.1 Minimum-energy crossing points (MECPs) along two different S_0/S_1 conical seams for the ethylene molecule, plotted as a function of orthogonalized \mathbf{g} and \mathbf{h} coordinates. These calculations were performed using SF-TDDFT and the resulting potential surfaces exhibit the correct double-cone topology of a CX. The intersection in (a) is strongly peaked whereas the one in (b) is more sloped. Energy is measured relative to the minimum-energy S_0 geometry. Reprinted from Ref. [37]; copyright 2016 American Chemical Society.

and the relationship is

$$\mathbf{d}_{JK}(\mathbf{R}) = \frac{\mathbf{h}_{JK}(\mathbf{R})}{E_K(\mathbf{R}) - E_J(\mathbf{R})}. \quad (10.6)$$

The derivative coupling describes the fact that the Born–Oppenheimer potential surfaces $E_J(\mathbf{R})$ and $E_K(\mathbf{R})$ are coupled due to nuclear motion, represented by the operator $\hat{\mathbf{V}}_{\mathbf{R}}$. The general solution to the coupled nuclear–electronic problem involves a

vibronic Schrödinger equation [11], rather than the purely electronic one in Eq. (10.3), the latter of which describes the uncoupled Born–Oppenheimer approximation. Unless $\partial \hat{H} / \partial x$ happens to vanish by symmetry along a particular coordinate x , then electronic states J and K will be strongly coupled in regions where the energy gap $|E_J(\mathbf{R}) - E_K(\mathbf{R})|$ is small.

The topography around a given CX (peaked versus sloped, and symmetrical versus ellipsoidal) can be characterized using parameters related to \mathbf{g}_{JK} , \mathbf{h}_{JK} , and a *seam coordinate*

$$\mathbf{s}_{JK} = \frac{1}{2} \hat{\nabla}_{\mathbf{R}} [E_J(\mathbf{R}) + E_K(\mathbf{R})]. \quad (10.7)$$

Omitting the subscript JK in cases where there is no ambiguity, and denoting $g = \|\mathbf{g}\|$ and $h = \|\mathbf{h}\|$, Yarkony [125] defines parameters

$$s^x = (\mathbf{s} \cdot \mathbf{g}) / g^2 \quad (10.8a)$$

$$s^y = (\mathbf{s} \cdot \mathbf{h}) / h^2 \quad (10.8b)$$

that describe the “tilt” of the CX. When s^x and s^y are small, the CX is strongly peaked or hourglass-shaped, as in Fig. 10.1a. Larger values of either s^x or s^y correspond to a more sloped CX in either the \mathbf{g} or the \mathbf{h} direction, respectively, as in Fig. 10.1b. Peaked CXs are generally understood to be better funnels [1], leading to more efficient nonadiabatic transitions. Note also that it is common to minimize the energy along the seam coordinate \mathbf{s}_{JK} , maintaining the degeneracy $E_J(\mathbf{R}) = E_K(\mathbf{R})$. This affords the *minimum-energy crossing point* (MECP) along the conical seam, which is sometimes characterized as “the” CX. Both of the intersection points that are plotted in Fig. 10.1 are MECPs along a particular conical seam.

10.1.2 Time-Dependent DFT

CXs can be appropriately described using a variety of (mostly multireference) electronic structure methods [73], but the present chapter focuses on their description using time-dependent density functional theory (TDDFT) [19, 32, 33] in its linear-response (LR) formulation [8, 18, 23]. The frequency-domain formulation of LR-TDDFT involves an eigenvalue problem for the excitation energies and no explicit time dependence, nevertheless that method is

nowadays largely synonymous with simply “TDDFT.” Explicitly time-dependent approaches do exist and their use is increasing [61], but these are not discussed in the present chapter. LR-TDDFT represents something of a “sweet spot” in terms of its price-to-performance ratio, with an accuracy of ~ 0.3 eV for many classes of vertical excitation energies [52, 91, 103], and a cost that scales as $n_{\text{states}} \times \mathcal{O}(n_{\text{basis}}^4)$, i.e., fourth-order scaling with a prefactor that reflects the number of desired states [24]. For many photochemical problems, only a few low-lying electronic states are required and the cost is not significantly greater than that of the ground-state DFT calculation.

That is the good news, and it has made LR-TDDFT absolutely ubiquitous for the calculation of vertical excitation spectra. The bad news, from the standpoint of photochemical investigations, is that the topology of any CX that involves the ground state is fundamentally flawed in LR-TDDFT, with seams that are $(N_{\text{int}} - 1)$ -dimensional rather than $(N_{\text{int}} - 2)$ -dimensional [37, 60]. This can be seen clearly from the LR-TDDFT potential energy surfaces for ethylene that are plotted in Fig. 10.2, around the same two geometries used to generate the plots in Fig. 10.1. Using LR-TDDFT, no intersection with the correct topology can be found. Numerical values of the tilt parameters in Eq. (10.8) also fail to correlate with the observed potential energy landscape [37].

This incorrect behavior originates in a lack of proper coupling between the ground (reference) state and the response (excited) states. At some level, this is a problem with response theory rather than with TDDFT *per se*, and from a different point of view the issue is that LR-TDDFT affords an unbalanced treatment of ground versus excited states. The ground state is variationally optimized via solution of the Kohn–Sham equations but then the excited states are obtained from a separate eigenvalue problem, and therefore do not satisfy a variational principle with respect to the ground state. (The excited states are, however, variational with respect to one another. As a result, CXs between two excited states are free of the aforementioned topology problems.) The predicament is brought to the forefront by Jahn–Teller problems involving symmetry-required degeneracy of the ground state, and the simplest such example is the H_3 radical in its D_{3h} geometry. As a result of the unbalanced manner in which ground and excited states are described, conventional LR-

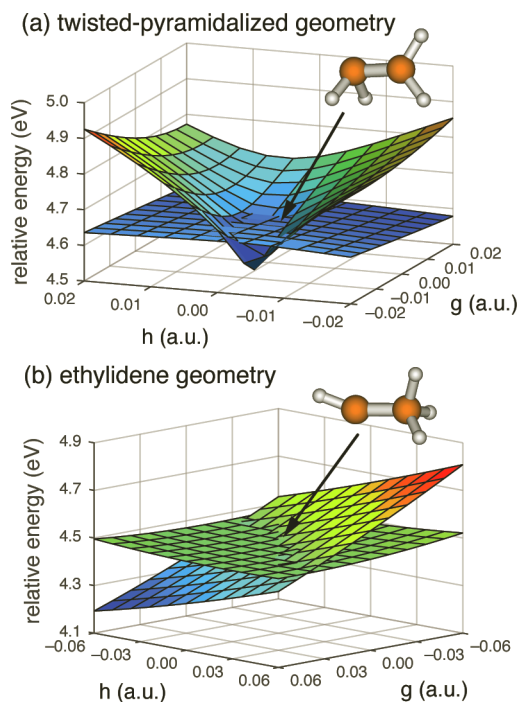


Figure 10.2 Potential surfaces for the S_0 and S_1 states of C_2H_4 , computed around the same two geometries that are depicted in Fig. 10.1 but this time using conventional LR-TDDFT. Nowhere in the vicinity of the known MECP structures does a CX (i.e., a zero-dimensional point of intersection) manifest, because LR-TDDFT exhibits fundamentally incorrect topology for any CX that involves the reference state, which is S_0 for these calculations. Reprinted from Ref. [37]; copyright 2016 American Chemical Society.

TDDFT struggles to describe the degeneracy [130], as can be seen clearly in Fig. 10.3b. To emphasize that this is not a DFT problem *per se*, Fig. 10.3a shows that the configuration interaction singles (CIS) method [18] also struggles, even in a restricted open-shell formulation.

Despite these drawbacks, LR-TDDFT has been formulated for use with nonadiabatic molecular dynamics methods [3, 16, 46, 108–110, 113]. It is sometimes found that the electronic structure calculation is difficult to converge in regions of the potential surface where the ground state is quasi-degenerate with the first excited

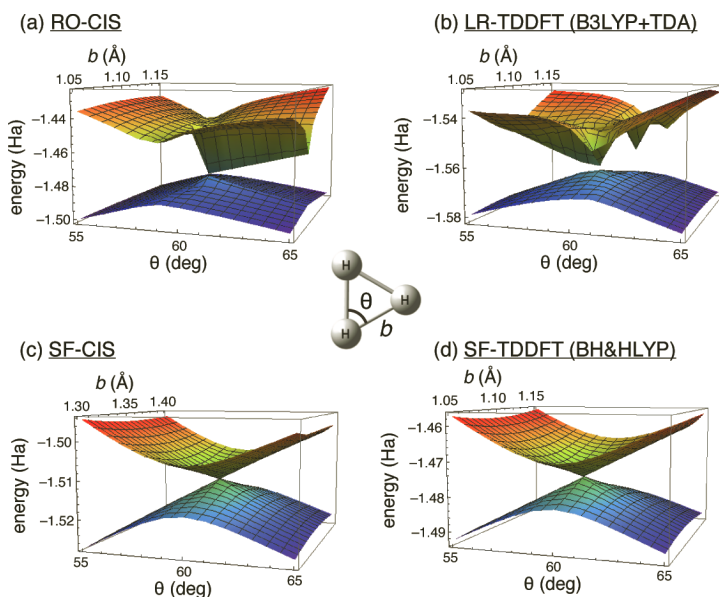


Figure 10.3 Potential energy surfaces for the lowest two doublet electronic states of H_3 radical, centered at the D_{3h} geometry with displacements along one bond-length coordinate (b) and one bond-angle coordinate (θ), as defined in the center diagram, which reduce the symmetry to C_{2v} . The methods considered are: (a) restricted open-shell (RO-)CIS, (b) unrestricted LR-B3LYP within the Tamm–Dancoff approximation (TDA), (c) SF-CIS, and (d) SF-BH&HLYP. Energies are in Hartree. Adapted from Ref. [130]; copyright 2014 American Institute of Physics.

state [128, 130], which is not altogether surprising given the warped topography of the potential surfaces for H_3 that is documented in Fig. 10.3a and Fig. 10.3b. A practical workaround is to halt any excited-state dynamics simulation before it can reach a ground-state CX [88, 134], using LR-TDDFT only to simulate excited-state dynamics and nonadiabatic transitions between excited states. That procedure, however, is at odds with the desire to perform first-principles simulations of the crucial excited-state deactivation step, leading to the onset of vibrational cooling on the ground state.

The present chapter describes a solution to these dilemmas based on the “spin-flip” (SF) approach to TDDFT [7, 37, 100]. The formalism of SF-TDDFT is described in Section 10.2 but the essential

idea is rather simple: we recognize that the shortcomings described above are limited to CXs that involve the reference state that is used in LR theory, which is typically the ground state but it need not be. SF-TDDFT uses a sacrificial reference state with a different spin multiplicity as compared to the target states of interest, e.g., a triplet reference is used to simulate singlet photochemistry or a quartet reference for the doublet H_3 radical. The change in multiplicity is accomplished via single excitations in conjunction with a single $\alpha \rightarrow \beta$ spin flip, so that states having the target multiplicity (including the ground state) appear in the excitation manifold and are described in a variational manner with respect to one another. This cures the topology problem [130]. (In fact, the double cones in Fig. 10.1 were generated using SF-TDDFT calculations.) In Fig. 10.3c, the SF-CIS approach repairs the incorrect RO-CIS description of the conical intersection in H_3 . Adding dynamical correlation, SF-TDDFT recovers a double cone as well; see Fig. 10.3d.

The SF approach is not a panacea and some problems do remain, most notably that it exacerbates spin contamination, which can make it difficult to identify the multiplicities of interest. These problems are described in Section 10.2 and some recently emergent solutions, based on augmented SF-type approaches, are discussed in Section 10.3.

10.2 Spin-Flip TDDFT Approach

10.2.1 Theory

We first provide a conceptual overview of SF-TDDFT (Section 10.2.1.1) before briefly reviewing the formalism of LR-TDDFT as a means to introduce the SF version in more detail (Section 10.2.1.2). A discussion of LR- and SF-TDDFT derivative couplings appears in Section 10.2.1.3.

10.2.1.1 Conceptual overview

As with other SF approaches [7], the basic idea behind SF-TDDFT is to use a high-spin ($M_S = S$) reference state whose total spin S is one

unit larger than the states of interest, whose spin quantum number is $S - 1$. A simple example for a (4e,4o) model is shown in Fig. 10.4. There, a triplet ($S = 1$) reference configuration is used to generate a singlet ($S = 0$) excitation manifold. For the proper qualitative description of a S_0/S_1 intersection, the minimal excitation space is labeled “o-o” in Fig. 10.4 and consists of excitations within the half-filled orbitals of the reference configuration, including de-excitations. (Notably, if the molecule in question has a singlet ground state then the lowest SF-TDDFT excitation energy starting from a triplet reference is negative.) The o-o space contains a closed-shell configuration that resembles S_0 . It also contains two open-shell determinants with $M_S = 0$, linear combinations of which will generate either an open-shell singlet (S_1) or else the $M_S = 0$ component of the triplet state, depending on whether these determinants are added (triplet) or subtracted (singlet). Lastly, the o-o space contains a determinant that is doubly excited with respect to S_0 , which provides coupling between S_0 and S_1 . The four determinants in the o-o space thus constitute a minimalist model that can describe the S_0/S_1 intersection correctly [60]. Notably, the doubly excited determinant that is required is not contained in the usual LR-TDDFT excitation manifold starting from a closed-shell S_0 reference state, because that excitation manifold consists of single excitations only. From another point of view, SF-TDDFT thus represents a cost-effective way to augment the LR-TDDFT excitation manifold with a certain subset of doubly excited determinants.

The SF-TDDFT excitation manifold also consists of determinants involving the virtual orbitals (“o-v” and “c-v” subspaces in Fig. 10.4), along with the “c-o” space of excitations between doubly occupied and singly occupied orbitals. Unlike the o-o space, none these other subspaces is spin-complete [133], meaning that they are missing one or more determinants needed to construct \hat{S}^2 eigenstates but which cannot be generated from the reference state via a single excitation combined with a single spin-flip. These are the subspaces that are responsible for spin contamination. We will return to this point later in this chapter.

Operationally, a SF-TDDFT calculation consists of a configuration-interaction (CI) calculation within the extended manifold of determinants generated by single excitations combined with $\alpha \rightarrow \beta$

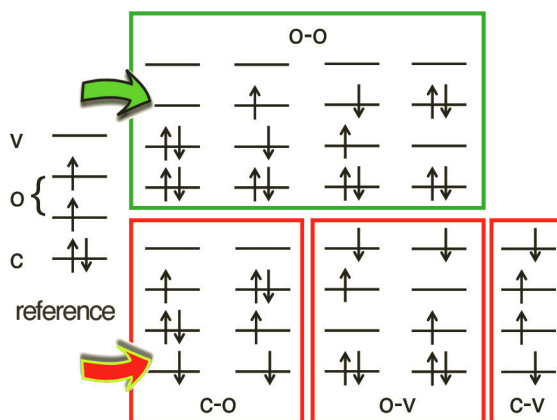


Figure 10.4 Illustration of the SF-TDDFT excitation space for a (4e,4o) model (i.e., four electrons in four orbitals), starting from a high-spin triplet reference at left. Single excitations combined with a single $\alpha \rightarrow \beta$ spin flip generate the determinants that are shown. The “o-o” set of determinants is spin-complete and represents a minimalist model of S_0 and S_1 along with the doubly excited determinant that couples them. Subspaces labeled c-o, o-v, and c-v are each missing some of the determinants needed to form spin-pure \hat{S}^2 eigenstates. Adapted from Ref. [133]; copyright 2015 American Institute of Physics.

spin flip. Unlike the SF-CIS method [49], however, the use of Kohn–Sham orbitals captures some dynamical correlation effects. Because the double excitations are limited, this CI problem does not incur the full $\mathcal{O}(N^6)$ cost of a singles-doubles (CISD) calculation, but rather is only a few times more expensive than conventional LR-TDDFT. The number of determinants in the excitation space remains $\mathcal{O}(N_{\text{occ}}N_{\text{virt}})$ [98], and does not grow in a way that increases with system size any faster than that of LR-TDDFT.

Crucially, this extension of the excitation manifold cures the topology problem around conical intersections involving any of the states of the target multiplicity, because the appropriate double excitation to couple them is included in the excitation manifold. Problems with symmetry-required (Jahn–Teller) degeneracy are mitigated, and the warped topography around such intersections is avoided (see Fig. 10.3), because both of the quasi-degenerate electronic states are treated on the same footing and emerge as

solutions to a common eigenvalue problem [130, 134]. Convergence problems around such regions of near-degeneracy are mitigated as well.

10.2.1.2 Formalism

To proceed let us recapitulate the form of the ground-state (Kohn-Sham DFT) and excited-state (LR-TDDFT) eigenvalue problems. The former is

$$\hat{F} \psi_{p\sigma}(\mathbf{r}) = \varepsilon_{p\sigma} \psi_{p\sigma}(\mathbf{r}), \quad (10.9)$$

which defines the molecular orbitals (MOs) $\{\psi_{p\sigma}\}$, where σ is a spin index. The excited-state eigenvalue problem is [18, 23]

$$\begin{pmatrix} \mathbf{A} & \mathbf{B} \\ \mathbf{B}^* & \mathbf{A}^* \end{pmatrix} \begin{pmatrix} \mathbf{x} \\ \mathbf{y} \end{pmatrix} = \omega \begin{pmatrix} \mathbf{1} & \mathbf{0} \\ \mathbf{0} & -\mathbf{1} \end{pmatrix} \begin{pmatrix} \mathbf{x} \\ \mathbf{y} \end{pmatrix} \quad (10.10)$$

where the matrices \mathbf{A} and \mathbf{B} involve derivatives of the ground-state Fock matrix \mathbf{F} with respect to the ground-state density matrix \mathbf{P} [18]:

$$A_{ia\sigma, jb\sigma'} = (\varepsilon_{a\sigma} - \varepsilon_{i\sigma}) \delta_{ij} \delta_{ab} \delta_{\sigma\sigma'} + \frac{\partial F_{ia\sigma}}{\partial P_{jb\sigma'}} \quad (10.11a)$$

$$B_{ia\sigma, jb\sigma'} = \frac{\partial F_{ai\sigma}}{\partial P_{jb\sigma'}}. \quad (10.11b)$$

The term $\partial F_{ia\sigma} / \partial P_{jb\sigma'}$ in \mathbf{A} , along with the entirety of \mathbf{B} , has the form of a coupling matrix that modifies the zeroth-order (independent-particle) excitation energies, $\varepsilon_{a\sigma} - \varepsilon_{i\sigma}$.

The solution of Eq. (10.10), for the l th excited state, consists of an excitation energy (eigenvalue) $\omega_l = E_l - E_0$, along with vectors \mathbf{x}^l and \mathbf{y}^l consisting of excitation amplitudes and de-excitation amplitudes, respectively. We will use indices i, j, \dots to denote occupied MOs and a, b, \dots for virtual MOs, and p, q, \dots for arbitrary MOs, as in the p that appears in Eq. (10.9). The solution vector (\mathbf{x}, \mathbf{y}) to Eq. (10.10) parameterizes the transition density $\rho_{0l}(\mathbf{r}, \mathbf{r}')$ of the excited state in question [23, 24, 105]:

$$\rho_{0l}(\mathbf{r}, \mathbf{r}') = \sum_{ia\sigma} \left[x_{ia\sigma} \psi_{a\sigma}(\mathbf{r}) \psi_{i\sigma}^*(\mathbf{r}') + y_{ia\sigma} \psi_{i\sigma}(\mathbf{r}) \psi_{a\sigma}^*(\mathbf{r}') \right]. \quad (10.12)$$

The de-excitation amplitudes y_{ia} , which appear in the random phase approximation as a correlation contribution to the ground

state [75, 92], and are typically $\sim 100\times$ smaller than the excitation amplitudes x_{ia} . Neglecting the $\{y_{ia}\}$, affords the so-called Tamm-Dancoff approximation (TDA) to Eq. (10.10) [18, 38]:

$$\mathbf{A}\mathbf{x} = \omega\mathbf{x}. \quad (10.13)$$

Equation (10.13) has the same form as the CIS eigenvalue equation except that the matrix elements contain a contribution from the exchange-correlation kernel, $f_{xc} = \delta^2 E_{xc}/\delta\rho^2$. In the LR-TDDFT case, the matrix elements are [18]

$$A_{ia\sigma, jb\sigma'} = (\varepsilon_a - \varepsilon_i)\delta_{ia}\delta_{jb}\delta_{\sigma\sigma'} + (ia|jb) - C_{\text{HFX}}(ij|ab)\delta_{\sigma\sigma'} + (1 - C_{\text{HFX}})(ia\sigma|f_{xc}|jb\sigma'). \quad (10.14)$$

The quantity C_{HFX} is the fraction of Hartree-Fock exchange (HFX), in the case that the functional is a hybrid.

The TDA is generally a very good approximation, but for photochemical applications its utility goes deeper than that. To understand why, consider that the full LR-TDDFT eigenvalue problem in Eq. (10.10) can be rewritten as

$$(\mathbf{A} - \mathbf{B})(\mathbf{A} + \mathbf{B})(\mathbf{x} + \mathbf{y}) = \omega^2(\mathbf{x} + \mathbf{y}), \quad (10.15)$$

where the matrices $\mathbf{A} \pm \mathbf{B}$ are orbital Hessians, i.e., stability matrices [123]. Solution of this equation for excitation energies ω will fail if the triplet instability matrix $\mathbf{A} + \mathbf{B}$ exhibits any negative eigenvalues. Such instabilities are found to be widespread once one an excited-state trajectory moves away from the Franck-Condon excitation point and begins to explore bond-breaking regions of the potential energy surface [14], leading to the suggestion that the TDA is effectively mandatory for photochemical applications.

The preceding discussion describes the conventional LR-TDDFT formalism, in which $x_{ia\sigma}$ has a single spin index because the $\psi_{i\sigma} \rightarrow \psi_{a\sigma}$ excitation is spin-conserving. For a spin-flipping transition, and under the usual assumption that f_{xc} comes from a semilocal exchange-correlation functional, the coupling matrix $\partial F_{ia\sigma}/\partial P_{jb\sigma'}$ in Eq. (10.11a) vanishes except for the HFX contribution [100], because only HFX can couple $\sigma = \alpha$ to $\sigma' = \beta$. As noted later [43], the fact that the SF-TDDFT coupling matrix involves only the HFX term (and not the Coulomb term or the semilocal kernel f_{xc}) explains the observation, made already in the very first SF-TDDFT study of

singlet–triplet gaps [100], that a hybrid functional with 50% HFX significantly outperforms B3LYP with its 20% HFX. This observation was later confirmed in application of SF-TDDFT to excitation energies [64]. As a result, the “Becke half-and-half” functional BH&HLYP, consisting of 50% HFX and 50% semilocal B88 [5] exchange (“BH&H”), in conjunction with LYP correlation [53], has become the standard choice for SF-TDDFT calculations.

The formulation of SF-TDDFT that is outlined above is sometimes called the “collinear” approach. This was later generalized to an alternative “noncollinear” method, which does bring the semilocal part of the functional into the coupling matrix [119, 120]. (See Refs. [43] and [89] for additional discussion of the noncollinear approach. The name comes from generalized Hartree–Fock theory [104], where a noncollinear formalism is one that allows α and β spin to mix, as used for example in relativistic DFT [25, 26, 118].) The noncollinear version of SF-TDDFT is found to improve the performance for some problematic diradicals [6, 120], and is more accurate for excitation energies when functionals with a low percentage of HFX are used [45, 124]. A significant drawback, however, is that the noncollinear exchange–correlation kernel involves a numerically problematic factor of spin density ($\rho_\alpha - \rho_\beta$) in the denominator [6, 89]. Likely for this reason, the noncollinear formulation is less widely used and is not discussed further in this chapter.

10.2.1.3 Nonadiabatic (derivative) couplings

To fully explore nonadiabatic photochemistry with TDDFT (or any other electronic structure method) it is necessary to possess not only an analytic gradient but also nonadiabatic coupling vectors \mathbf{h}_{JK} [Eq. (10.2)]. As compared to the gradient, the couplings are more complicated to derive and implement, and as a result they are available only in selected quantum chemistry programs and only for a limited number of electronic structure models, which includes TDDFT. A survey of implementations can be found in Ref. [3], although it omits the implementation in the Q-Chem program [50]. The latter is the joint product of the Herbert group [130, 132] and

the Subotnik group [21, 46, 84]. Semi-empirical implementations have also been reported recently [68, 81].

Out of a variety of formalisms for computing nonadiabatic couplings within TDDFT [12, 99, 112, 130, 132], the one that is conceptually and computationally simplest is the “pseudo-wavefunction” approach [21, 84, 130]. Working within the TDA, both for conceptual simplicity and for the practical reasons discussed above, one might write the wavefunction for the K th excited state as a linear combination of singly excited Slater determinants, as in the CIS method:

$$|\Psi_K\rangle = \sum_{i\alpha\sigma} x_{i\alpha\sigma}^K |\Phi_{i\alpha\sigma}\rangle. \quad (10.16)$$

Here, $|\Phi_{i\alpha\sigma}\rangle$ is obtained from the ground state configuration by $\psi_{i\sigma} \rightarrow \psi_{\alpha\sigma}$ excitation. Strictly speaking, LR-TDDFT affords only the transition density $\rho_{0K}(\mathbf{r}, \mathbf{r}')$ [Eq. (10.12)], not the excited-state wavefunction *per se*, but analogies along the lines of Eq. (10.16) have been used since the earliest days of the theory [8–10, 96]. In condensed-matter physics, it is also common to identify the product functions $\psi_a(\mathbf{r}_{\text{elec}}) \psi_i^*(\mathbf{r}_{\text{hole}})$ as a quasiparticle basis for electron-hole pairs (“excitons”), and to consider $\rho_{0K}(\mathbf{r}_{\text{elec}}, \mathbf{r}_{\text{hole}})$ to be an “exciton wavefunction” [90, 101]. This is despite the fact that the Green’s function methods that are often used in that context afford transition densities rather than proper wavefunctions, just like LR-TDDFT.

Taking Eq. (10.16) as an *ansatz* for the excited-state wavefunction, analytic expressions can then be derived for \mathbf{h}_{JK} using standard analytic gradient theory, which essentially means careful application of the chain rule [21, 84, 130]. The relevant expressions will not be repeated here; see Zhang and Herbert for a concise derivation [130] and for a generalization beyond the TDA [132]. The results are in good agreement with derivative couplings computed via quadratic response theory [132], which is the formally correct way to obtain \mathbf{h}_{JK} within TDDFT [83, 86], at least when quadratic response is well-behaved. That method, however, is vulnerable to spurious divergences [67, 83, 86, 132], a fact that was actually noted long ago in the context of time-dependent Hartree–Fock theory [17]. As explained later by Furche and co-workers [87], these are artifacts of approximate response theory in general, not limited to TDDFT,

and they complicate the application of quadratic response to the point that the pseudo-wavefunction approach is the much more widely used method. Similarly, the topology problem around a CX is not unique to LR-TDDFT and is also an artifact of response theory, and in particular the unbalanced (and nonvariational) manner in which it treats the reference and response states. Correlated Green's functions methods also afford wrong topology at any CX involving the reference state, whereas SF versions of those methods restore the correct topology [58].

Derivative couplings computed within the pseudo-wavefunction formalism show good agreement with exact (full CI) results for small molecules [132], good agreement with LR theory for derivative couplings \mathbf{d}_{0K} that involve the ground state [83], and (for couplings between two excited states) good agreement with quadratic response theory [83, 132], provided that the latter is well-behaved. Some exemplary data are shown in Fig. 10.5, where derivative couplings \mathbf{d}_{JK} computed within the pseudo-wavefunction approach are compared to results from quadratic response theory for a set of small molecules, and also to exact (full CI) results for linear H_3 as a function of internuclear distance. Derivative couplings based on the pseudo-wavefunction formalism also correctly reproduce the branching plane and the Berry phase around a CX [82], for which the orbital response contributions to \mathbf{d}_{JK} prove to be crucial. Results presented below demonstrate that MECs located with the aid of pseudo-wavefunction \mathbf{h}_{JK} vectors afford good agreement with benchmark results from multireference electronic structure methods. Within the TDA, the pseudo-wavefunction formalism also affords the same result for \mathbf{d}_{JK} as does the equation-of-motion formalism developed by Li and Liu [65]. All of these features argue in favor of using the pseudo-wavefunction approach, to the exclusion of quadratic response theory.

A subtle aspect of the derivative couplings is that of translational invariance. As noted by Fatehi et al. [21], expressions for \mathbf{h}_{JK} obtained from straightforward application of the pseudo-wavefunction approach are not translationally invariant, which is problematic for nonadiabatic molecular dynamics simulations [22], and certain "electronic translation factors" were introduced to restore translational invariance [21]. It was noted that the terms

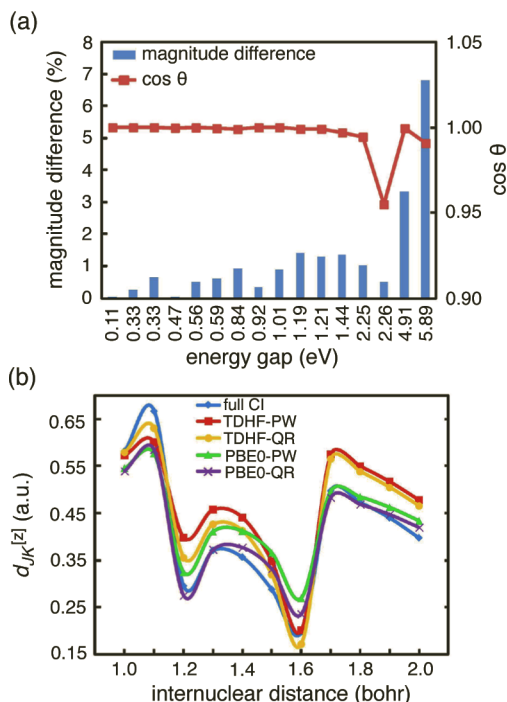


Figure 10.5 (a) Differences between \mathbf{d}_{JK} computed using the pseudo-wavefunction (PW) approach versus quadratic response (QR) theory, expressed both in terms of magnitude $\|\mathbf{d}_{JK}^{\text{PW}} - \mathbf{d}_{JK}^{\text{QR}}\|$ and also direction ($\cos \theta$, where θ is the angle between $\mathbf{d}_{JK}^{\text{PW}}$ and $\mathbf{d}_{JK}^{\text{QR}}$). Results correspond to S_1/S_2 and S_1/S_3 couplings for formaldehyde, ethene, benzene, adenine, thymine, uracil, cytosine, and azulene. The energy gap axis consists of the individual gaps for this set of molecules and states. (b) Derivative coupling between the lowest ${}^2\Sigma_g^+$ states of linear H_3 radical ($D_{\infty h}$ symmetry) as a function of internuclear distance. Reproduced from Ref. [132]; copyright 2015 American Institute of Physics.

violating translational invariance arise from a kind of “Pulay force” [36], meaning derivatives of the overlap matrix in an atom-centered Gaussian basis set. It was later demonstrated by Zhang and Herbert [130] that the electronic translation factors introduced in Ref. [21] precisely annihilate the non-Hellmann–Feynman parts of \mathbf{h}_{JK} . The translationally invariant Hellmann–Feynman expression is

easy to state, at least in schematic form [130]. Within the TDA, it is

$$h_{JK}^{[x]} = \sum_{ia} \sum_{jb} \sum_{\sigma, \sigma'} x_{ia\sigma}^J A_{ia\sigma, jb\sigma'}^{[x]} x_{jb\sigma'}^K, \quad (10.17)$$

where the superscript $[x]$ indicates a derivative with respect to the nuclear coordinate x , as in Eq. (10.4b). The quantity $A_{ia\sigma, jb\sigma'}^{[x]}$ involves derivatives of the integrals in Eq. (10.14).

As will be discussed below, analytic derivative coupling vectors are useful for nonadiabatic molecular dynamics simulations. The \mathbf{h}_{JK} vectors are also very useful for locating MECPs, because they facilitate the use of more efficient branching-plane updating methods [4, 102], in which the branching space (spanned by \mathbf{g}_{JK} and \mathbf{h}_{JK}) is projected out of the gradient so that optimization proceeds entirely within the seam space. As compared to MECP-optimization algorithms that do not require \mathbf{h}_{JK} vectors, such as penalty-function methods [59, 78] or approximate branching-plane updating [70, 131], the use of an *exact* branching-plane updating method requires far fewer optimization steps [48, 130, 131]. When programmed efficiently, evaluation of \mathbf{h}_{JK} requires only modest overhead on top of the TDDFT gradient calculation that is already required to compute $\hat{\mathbf{V}}_R E_J$ and $\hat{\mathbf{V}}_R E_K$, because solution of coupled-perturbed equations is required in either case. Timing data confirm that the overhead for computing \mathbf{h}_{JK} amounts to no more than 10–20% on top of the cost of TDDFT analytic gradients [99, 130].

10.2.2 Photochemical Applications

Although it can be tempting to jump right into nonadiabatic molecular dynamics simulations (which are discussed in Section 10.2.2.2), those simulations can be quite expensive because energy conservation typically requires time steps $\Delta t = 0.5\text{--}1.0$ fs, and accurate integration of the couplings (which vary rapidly in regions where energy gaps are small) may require even smaller time steps. Moreover, the results of such simulations are generally meaningful only in the aggregate, i.e., when averaged over an ensemble of trajectories. It may therefore be useful to first locate critical points on the potential energy surface, such as excited-state local minima and MECPs between electronic states, the latter of which not only

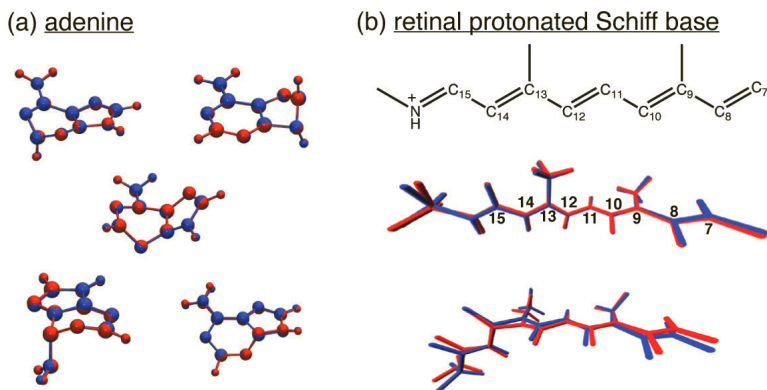


Figure 10.6 Comparison of optimized MECP structures obtained using SF-BH&HLYP to benchmark results from multireference electronic structure methods. (a) Comparison against MR-CIS for five different MECPs of adenine. (b) Comparison against CASSCF results for two MECPs of a truncated model of the rhodopsin chromophore, corresponding to *trans* → *cis* isomerization around either $C_{11}=C_{12}$ or $C_{13}=C_{14}$. Panel (a) is adapted from Ref. [131]; copyright 2014 American Chemical Society. Panel (b) is adapted from Ref. [37]; copyright 2016 American Chemical Society.

indicate where the photochemical funnels are found in coordinate space, but also which vibrational modes provide the strongest coupling between the electronic states in question. Examples of MECP optimization are presented in Section 10.2.2.1.

10.2.2.1 Exploring excited-state potential surfaces

Figure 10.6 presents some examples of MECPs optimized using SF-TDDFT (with the BH&HLYP functional) in comparison to results from multireference electronic structure methods. In each case, the MECP obtained using SF-TDDFT is nearly indistinguishable from the benchmark multireference result. The test set includes five MECPs for adenine and two MECPs for a truncated model of the retinal protonated Schiff base that functions as the chromophore in the rhodopsin photoreceptor protein [20]. In retinal, *trans* → *cis* photoisomerization occurs around a different double bond in solution [117] ($C_{13}=C_{14}$) than it does in the protein environment

($C_{11}=C_{12}$) [20], and the structures in Fig. 10.6b include MECPs for both isomerization reactions. Additional comparisons in Ref. [44] also indicate that SF-TDDFT accurately predicts MECP geometries.

Although applications of SF-TDDFT have been somewhat limited to date, the method has been used to map out potential energy surfaces and/or locate critical points for a variety of small molecules, including both uracil [131] and thymine [77], where the goal in both cases was to rationalize observed differences between the excited-state lifetime in the gas phase versus that in aqueous solution. Detailed photoisomerization pathways have also been mapped out for *cis* \rightarrow *trans* photoisomerization in stilbene [78], and for the photochemical ring-opening of cyclohexadiene [95]. The method has been combined with exhaustive search algorithms in an attempt to elucidate all of the critical points (minima, transition states, and MECPs) for the S_0 and S_1 states of ethylene, 1,3-butadiene, thymine, and a coumarin dye [35, 69].

10.2.2.2 Trajectory surface hopping

Excited-state, nonadiabatic molecular dynamics simulations are mostly based on trajectory surface hopping (TSH) methods [2, 3, 47, 80, 106, 121, 122], most of which derive from Tully's seminal "fewest switches" algorithm [114], although modern variants incorporate some level of decoherence effects that are absent in Tully's original method [106, 121]. A notable exception (not based on Tully's algorithm) is the "multiple spawning" approach of Martínez and co-workers [15], which is an approximation to quantum wavepacket dynamics. The discussion below regarding the need for derivative coupling vectors is relevant to all of these methods. An example of a nonadiabatic dynamics algorithm that does *not* require derivative couplings is Zhu's "global switching" algorithm [126, 129], which derives from Landau-Zener theory. It is worth recalling (as discussed above) that properly coded TDDFT derivative couplings require only 10–20% additional computational overhead on top of a TDDFT analytic gradient calculation [99, 130]. Furche and co-workers report that TDDFT-based TSH simulations of the photodynamics of thymine, including the lowest three electronic states, require

only $5\times$ the cost of ground-state Born–Oppenheimer molecular dynamics, even with explicit calculation of derivative couplings [88]. As such, the discussion here focuses on the more popular TSH-based approaches and it is assumed that vectors \mathbf{d}_{JK} are available for all pairs JK of energetically accessible states.

In one way or another, TSH methods derive from the time-dependent Schrödinger equation of motion for the coefficients C_K of the electronic states in a superposition $|\Psi(t)\rangle = \sum_K C_K(t)|\Psi_K\rangle$. In the adiabatic basis $\{|\Psi_K\rangle\}$ of Born–Oppenheimer electronic states, the foundational equation of motion is usually [114, 121]

$$i\hbar \frac{dC_J}{dt} = E_J(\mathbf{R})C_J - i\hbar \sum_{K \neq J} C_K \dot{\mathbf{R}} \cdot \mathbf{d}_{JK} \quad (10.18)$$

where $\dot{\mathbf{R}}$ is the nuclear velocity vector. Clearly, it is the derivative coupling \mathbf{d}_{JK} that is responsible for stimulating transitions between electronic states. See Ref. [27] for a discussion regarding the absence of second-order derivative couplings in Eq. (10.18).

Derivative couplings are defined as

$$d_{JK}^{[x]} = \langle \Psi_J | (\partial/\partial x) | \Psi_K \rangle \quad (10.19)$$

and these are only available in a limited number of quantum chemistry programs and only at selected levels of theory. More generally, the term that includes \mathbf{d}_{JK} in Eq. (10.18) can be recast as

$$\dot{\mathbf{R}} \cdot \mathbf{d}_{JK} = \left\langle \Psi_J \left| \frac{d\Psi_K}{dt} \right. \right\rangle \approx \frac{\langle \Psi_J(t) | \Psi_K(t + \Delta t) \rangle}{\Delta t}, \quad (10.20)$$

where the first equality is exact but the second represents a finite-difference approximation that allows the coupling term in Eq. (10.18) to be evaluated by determining the overlap (in time) of the adiabatic basis functions [94]. While the approximation in Eq. (10.20) is numerically advantageous as compared to approximating Eq. (10.19) via finite differences involving coordinate displacements, even the more efficient finite-difference in time is less desirable as compared to analytic evaluation of \mathbf{d}_{JK} .

There have so far been only a few TSH studies using SF-TDDFT. Yue et al. [127] used this approach to make a first-principles investigation of the mechanism of firefly bioluminescence, specifically, the

photoinitiated decomposition reaction to form the anionic emitter species, oxyluciferin. Nakai and co-workers recently implemented SF-TDDFT at the level of semi-empirical density-functional tight-binding (“DFTB”) [115, 116], and have used the method to perform TSH simulations of the archetypal azobenzene photoisomerization, in explicit solvent [116]. Lastly, Minezawa and Nakajima have simulated S_1 lifetimes for several small molecules [79], demonstrating good agreement with previous TSH simulations employing multireference electronic structure methods. That study recognizes that because LR-TDDFT may skew the topology of CXs that involve the ground state, TSH simulations that employ LR-TDDFT ought to be terminated prior to the final internal conversion step that returns the molecule to its ground state. If this paradigm is followed then S_1 lifetimes are inaccessible to LR-TDDFT simulations, whereas SF-TDDFT suffers no such limitation.

Along these lines, two recent TSH studies have made a side-by-side comparison of S_1 lifetimes predicted by LR- versus SF-TDDFT. Zhu and co-workers [128] examined *cis* \rightarrow *trans* photoisomerization of azobenzene and found little difference between either the predicted S_1 lifetime or the branching ratio between *cis* and *trans* photoproducts, at odds with the notion that topology of the S_0/S_1 CX should lead to differences in measurable observables. It is certainly true that most nonadiabatic transitions happen *near* rather than *at* a CX, if only because the volume of configuration space is much larger if one admits quasi-degenerate geometries. It is therefore possible that in some cases the topological details may have no observable impact on the outcome of a particular photochemical reaction. A contrasting example, however, comes from a recent TSH study of the *trans* \rightarrow *cis* photoisomerization of the protonated Schiff base $C_5H_6NH_2^+$, for which LR- and SF-TDDFT methods predict significantly different S_1 lifetimes [134]. The lifetime predicted using SF-TDDFT agrees with that obtained in CASPT2-based TSH simulations, whereas the LR-TDDFT lifetime is much longer. The reason is that topological problems in LR-TDDFT warp the S_1 potential surface in the vicinity of the photochemically relevant S_0/S_1 intersection, leading to the presence of a barrier that is not present in either the SF-TDDFT calculations or the multireference benchmarks [134]. LR-TDDFT’s topology problem thus manifests as

a *topography* problem, and trapping behind an artificial barrier leads to slower dynamics. Such problems appear to manifest in some but not all cases, e.g., LR-TDDFT potential energy surfaces for CH_2NH_2^+ are reported to be in good agreement with multireference results in the region of an S_0/S_1 intersection [111]. Results for $\text{C}_5\text{H}_6\text{NH}_2^+$ as well as theoretical considerations, however, demonstrate that there is a potential for serious problems.

It is also notable that in the azobenzene simulations reported in Ref. [128], a significant fraction of the LR-TDDFT trajectories had to be terminated and discarded due to convergence failure in the region of quasi-degeneracy, whereas none of the SF-TDDFT trajectories suffered this problem. This is likely a direct result of the more balanced treatment of the two states in the SF approach. Furthermore, the time-dependent energy gap $E_1 - E_0$ is observed to be much more oscillatory in the LR-TDDFT simulations, leading to much more frequent hopping events and concomitant oscillations in the populations of the two electronic states [128]. At the SF-TDDFT level, the energy gap is less oscillatory, the population dynamics are smoother, and hopping events are relatively infrequent [128].

10.2.2.3 Spin contamination and state tracking

While SF-TDDFT rigorously cures the topology problem around CXs, it tends to significantly worsen the spin contamination as compared to LR-TDDFT, because some double excitations are admitted into the excitation space but not in a manner that introduces all of the complementary determinants needed to form spin-pure \hat{S}^2 eigenstates. In the (4e,4o) example of Fig. 10.4, the o-o subspace in spin-complete and contains a minimalist description of the S_0/S_1 intersection, however the remaining subspaces lack some of the determinants needed to form \hat{S}^2 eigenstates. Any excited state that contains significant contributions from outside the o-o subspace is likely to exhibit significant spin contamination. It is possible to minimally augment the excitation space to restore spin symmetry, and this approach has been used to construct a spin-complete version of SF-CIS [98]. Notably, this can be done without increasing the formal complexity of the method; the number of determinants

remains $\mathcal{O}(N_{\text{occ}}N_{\text{virt}})$, albeit with a somewhat larger prefactor as compared to conventional CIS. More automated versions of this approach are discussed in Section 10.3, including methods that incorporate a DFT treatment of dynamical correlation.

For practical application of the standard SF-TDDFT approach, especially for TSH simulations, it is necessary to use some kind of “state tracking” procedure that attempts to identify the best approximate multiplicity in regions of heavy spin contamination. Spin contamination tends to be relatively small near the ground-state geometry (Franck–Condon excitation point), whereas it becomes severe in bond-breaking regions of the potential surface where singlet and triplet states may be quasi-degenerate and therefore extensively mixed, in the absence of proper spin symmetry. A practical workaround is to categorize states based on their similarity to the wavefunctions computed in the previous time step, with the idea that spin multiplicities are identifiable at $t = 0$ so that the multiplicity of $|\Psi_K(t + \Delta t)\rangle$ can be assigned based on its overlap with the states $\{|\Psi_J(t)\rangle\}$. Several methods along these lines have been suggested [13, 34, 133]. The use of such algorithms is not guaranteed to lead to an unambiguous identification of the states in question, but it has been used successfully in TSH simulations [34].

10.3 Augmented Spin-Flip Methods

In the final section of this chapter, we introduce some methods that go beyond the simple SF *ansatz* in an attempt to correct some of its problems, most notably spin contamination. One of these is a spin-complete version of SF-TDDFT [133], which minimally augments that method’s excitation space in order to obtain a set of determinants from which spin-pure \hat{S}^2 eigenfunctions can be constructed. This is accomplished in an automated way using a tensor equation-of-motion (TEOM) formalism, as described in Section 10.3.1. An alternative approach is the “mixed reference spin-flip” (MRSF) procedure developed recently by Filatov, Choi, and co-workers [54], which is discussed in Section 10.3.2.

10.3.1 Spin-Adapted Spin-Flip Approach

10.3.1.1 Formalism

Originally developed from a wavefunction point of view [98], spin-complete SF-CIS lacks dynamical correlation but that shortcoming can be overcome using a TEOM framework to re-derive this method within the framework of TDDFT [133]. The TEOM formalism itself was originally developed in nuclear physics [93], but later extended to molecular systems by Li and Liu [62, 63, 66]. As applied to TDDFT, the result is a “spin-adapted” (SA-)SF-TDDFT method that maintains SF-TDDFT’s correct treatment of the topology around CXs but restores spin multiplicity as a good quantum number.

In SA-SF-TDDFT, excitation operators in the TEOM formalism are truncated at the single excitation level. The single-excitation operators can be grouped into two categories: those with zero rank (singlet coupling) and those with rank one (triplet coupling). Because SF methods use a target state of lower spin angular momentum as compared to the reference state, only the triplet-coupled excitation operators are useful in this case. These can be represented in the MO basis as

$$\hat{O}_{pq}^\dagger(1, 1) = -\hat{a}_p^\dagger \hat{a}_{\bar{q}} \quad (10.21a)$$

$$\hat{O}_{pq}^\dagger(1, 0) = (\hat{a}_p^\dagger \hat{a}_q - \hat{a}_{\bar{p}}^\dagger \hat{a}_{\bar{q}}) / \sqrt{2} \quad (10.21b)$$

$$\hat{O}_{pq}^\dagger(1, -1) = \hat{a}_{\bar{p}}^\dagger \hat{a}_q \quad (10.21c)$$

where \hat{a}_p^\dagger creates an α -spin electron in orbital ψ_p and $\hat{a}_{\bar{q}}$ annihilates a β -spin electron in orbital $\psi_{\bar{q}}$. Previous work by Li and Liu [62] uses a different working equation as a TEOM as compared to that used in SA-SF-CIS and SA-SF-DFT [133], and that equation generates spurious solutions due to the presence of redundant terms in the excitation space. The working equation used by Zhang and Herbert for SA-SF-TDDFT avoids this problem. The overall tensor operator can be written as

$$\begin{aligned} \hat{O}^\dagger(1) = & \sum_{ia} \hat{o}_{ia}^\dagger(1) x_{ia}^{cv} + \sum_{iu} \hat{o}_{iu}^\dagger(1) x_{iu}^{co} + \sum_{ua} \hat{o}_{ua}^\dagger(1) x_{ua}^{ov} \\ & + \sum_{tu} \hat{o}_{tu}^\dagger(1) x_{tu}^{oo} + \sum_{ai} \hat{o}_{ai}^\dagger(1) y_{ia}^{cv} \\ & + \sum_{ui} \hat{o}_{ui}^\dagger(1) y_{iu}^{co} + \sum_{au} \hat{o}_{au}^\dagger(1) y_{ua}^{ov}. \end{aligned} \quad (10.22)$$

As in conventional TDDFT, x_{ia} and y_{ia} are excitation and de-excitation amplitudes, respectively, with superscripts corresponding to the various subspaces in Fig. 10.4. For example, x_{ia}^{cv} is a coefficient from doubly occupied MO ψ_i to empty (virtual) MO ψ_a . Indices t and u in Eq. (10.22) are used to indicate singly occupied MOs.

The above SA-SF formalism can be used to generate a spin-complete version of SF-CIS. To extend this to DFT in a formally exact manner, it would be necessary to introduce a Hamiltonian \hat{H}^{DFT} that generates the exact ground-state energy as the expectation value of the single-determinant reference state. No such Hamiltonian is known in analytical form, so dynamical correlation is instead introduced as an *ad hoc* DFT correction to the SA-SF-CIS matrix elements, in a manner that is reminiscent of the *ad hoc* correction introduced in the DFT/MRCI method [31, 72]. The final matrix elements for SA-SF-DFT have the form

$$\begin{aligned} \langle \Phi_{pq} | \hat{H}^{\text{DFT}} - E_0^{\text{DFT}} | \Phi_{rs} \rangle = & \delta_{qs} F_{pr} - \delta_{pr} F_{qs} + \langle pq || qp \rangle \\ & + (1 - C_{\text{HFX}}) \langle pq | pq \rangle . \end{aligned} \quad (10.23)$$

This ends up being precisely the same matrix element as that used in collinear SF-TDDFT [130], which rationalizes the good performance of the method. In conjunction with Kohn–Sham orbitals determined via ground-state DFT, the extra determinants that are introduced to make the excitation manifold spin-complete do incur some double-counting of electron correlation effects, although one may argue this is likely to be small because the number of additional determinants is rather limited. In fact, the same issue arises in DFT/MRCI, where the overcounting is potentially more severe, and in that approach an empirical damping factor is introduced for the off-diagonal matrix elements in order to limit the scope of the double counting. A similar modification may help the SA-SF-DFT method, but has not yet been tested.

10.3.1.2 Applications

Eliminating the need for failure-prone state-tracking algorithms is crucial in order to make SF-TDDFT into a robust, black-box engine for TSH simulations, but elimination of spin contamination has practical consequences for excited-state optimizations and MECP

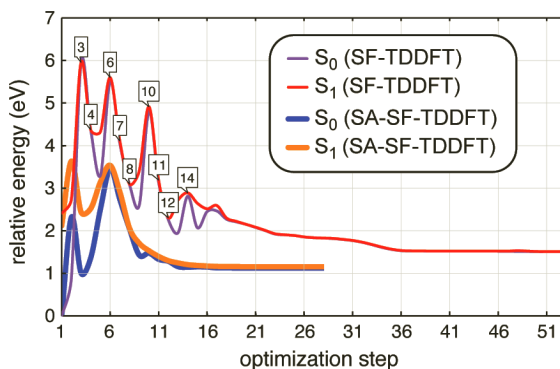


Figure 10.7 Optimization trajectories for a S_0/S_1 MECP of C_2H_4 , starting from the ground-state geometry and using either SF-TDDFT or SA-SF-TDDFT with the BH&HLYP functional. In the SF-TDDFT case, flags at steps 3, 4, 6, 7, ... indicate geometries at which the assignment of spin multiplicities becomes ambiguous due to spin contamination. Data are taken from Ref. [133].

searches. An example of the latter, for an S_0/S_1 MECP of ethylene, is presented in Fig. 10.7 in the form of an “optimization trajectory,” i.e., a plot of energy (for both S_0 and S_1) versus optimization steps. Using conventional SF-TDDFT, singlet and triplet states quickly become mixed so that already by the third optimization step it is difficult to assign spin multiplicities based on the value of $\langle \hat{S}^2 \rangle$ alone. At the third step, the two lowest-energy states have $\langle \hat{S}^2 \rangle = 1.14$ and $\langle \hat{S}^2 \rangle = 0.90$ (in units of \hbar^2), indicating nearly equal mixing of singlet and triplet [133]. Flags on steps 3, 4, 6, 7, 8, ... in Fig. 10.7 indicate points at which the state assignment is ambiguous. Energies of the two selected adiabats are strongly oscillatory, suggesting that the algorithm may be switching between states with differing amounts of singlet character, confounding the optimization algorithm. In contrast, the SA-SF-TDDFT optimization proceeds relatively smoothly and converges in far fewer steps. It is worth noting, however, that no analytic gradient has yet been reported for SA-SF-TDDFT, so MECP optimizations at that level of theory are proof-of-concept exercises based on finite-difference gradients [133].

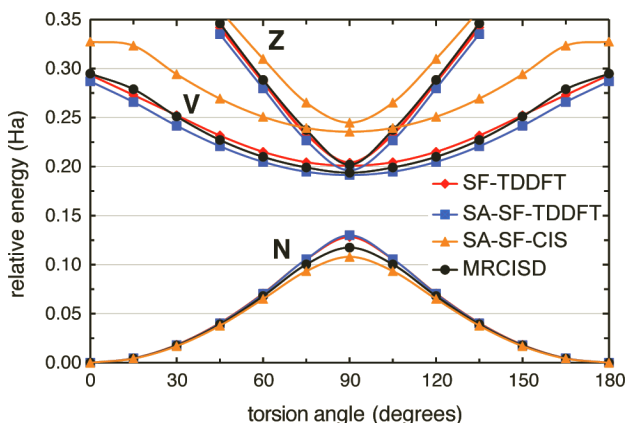


Figure 10.8 Potential energy curves along the C–C twisting coordinate for the lowest three singlet states of ethylene: N for the “normal” ground state or $(\pi)^2$ configuration, V for “valence” $(\pi)^1(\pi^*)^1$ state, and Z for “zwitterionic” $(\pi^*)^2$ state. (The notation is historical [76].) Reprinted from Ref. [133]; copyright 2015 American Institute of Physics.

As a second example of SA-SF-TDDFT, we consider the classic strong correlation problem of twisting C_2H_4 about its C–C axis. The $(\pi)^2$ and $(\pi^*)^2$ electron configurations become degenerate at a twist angle of 90° , causing single-reference methods based on spin-restricted orbitals to exhibit an unphysical cusp [51, 100]. Potential energy surfaces for the lowest three singlet states are plotted in Fig. 10.8, computed using several different SF methods and compared to a multireference benchmark. Both the simple SF-TDDFT method as well as SA-SF-TDDFT afford reasonably good agreement with the benchmarks for all three of the lowest singlet states, with no unphysical cusps. SA-SF-CIS results are also free of cusps although the absence of dynamical correlation causes the S_1 and S_2 surfaces to deviate significantly from the benchmarks.

10.3.2 Mixed-Reference Spin-Flip Approach

The MRSF approach to TDDFT has emerged recently as an alternative way to eliminate spin contamination in SF-TDDFT [54], if not rigorously and exactly (as in SA-SF-TDDFT) then at least to good numerical accuracy, without significantly increasing the

complexity with respect to the original method SF-TDDFT method. In Section 10.3.2.1, we briefly explain how MRSF-TDDFT works in the case where states of singlet multiplicity are targeted starting from a triplet reference state, and then a few exemplary applications are discussed in Section 10.3.2.2.

10.3.2.1 Formalism

MRSF-TDDFT is based on a mixed-reference (MR) state whose density matrix is a linear combination of the $M_S = 1$ and $M_S = -1$ components of a triplet reference state:

$$\rho_0^{\text{MR}}(\mathbf{r}, \mathbf{r}') = \frac{1}{2} \left[\rho_0^{M_S=+1}(\mathbf{r}, \mathbf{r}') + \rho_0^{M_S=-1}(\mathbf{r}, \mathbf{r}') \right]. \quad (10.24)$$

The two components of this density matrix are subjected to separate spin-flipping operations, $\alpha \rightarrow \beta$ for the $M_S = 1$ component (as in the basic SF-TDDFT method discussed above) and $\beta \rightarrow \alpha$ for the $M_S = -1$ component. This is shown schematically in Fig. 10.9 for the same (4e,4o) model that was used to introduce the basic method, using the same notation is used for the various subspaces of Slater determinants. Comparing Fig. 10.4 to Fig. 10.9, it is evident that MRSF-TDDFT introduces many more electronic configurations as compared to SF-TDDFT. Operationally, this removes the majority of the spin contamination even though the excitation space is not formally spin-complete because some of the necessary o-v determinants (shown in gray in Fig. 10.9) cannot be generated by this procedure. However, these are higher-energy configurations and thus play little role in low-lying excited states, so that $\langle \hat{S}^2 \rangle$ is close to its spin-pure value in practice [54].

Derivation of MRSF-TDDFT is based on the density matrix formulation of the time-dependent Kohn–Sham methodology [32, 33], which means that the density matrix needs to be idempotent. This can be demonstrated for the density matrix in Eq. (10.24) based on a complex rotation of the spin functions [54]. Separation of the $M_S = 1$ and $M_S = -1$ triplet density matrices leads to two independent eigenvalue equations,

$$\mathbf{A}_t \mathbf{x}_t = \omega_t \mathbf{x}_t \quad (10.25a)$$

$$\mathbf{A}_s \mathbf{x}_s = \omega_s \mathbf{x}_s. \quad (10.25b)$$

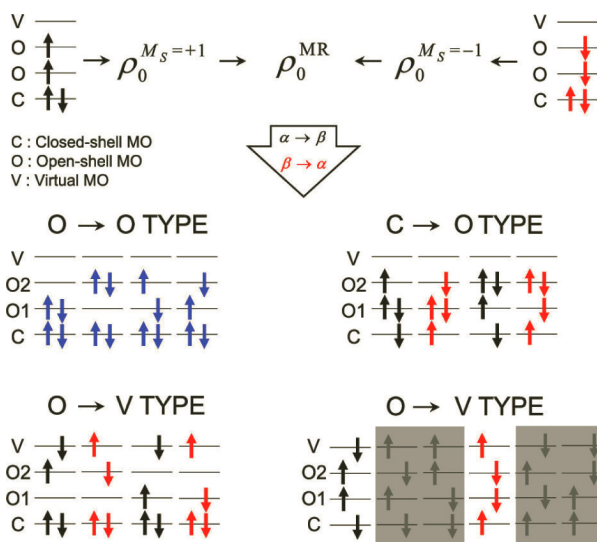


Figure 10.9 Schematic illustration of MRSF-TDDFT for a (4e,4o) model. The excitation space for singlet states is generated starting from both high- and low-spin triplet configurations, via single excitations combined with either $\alpha \rightarrow \beta$ spin flip (for $M_S = 1$) or $\beta \rightarrow \alpha$ spin flip (for $M_S = -1$). The four determinants shown in gray in the o-v subspace are missing from the excitation manifold because they cannot be generated in this manner. Adapted from Ref. [41]; copyright 2021 American Chemical Society.

However, it is necessary to incorporate coupling matrix elements between determinants from the $M_S = 1$ and $M_S = -1$ parts of the calculation on an *ad hoc* basis [54]. This amounts to new contributions to the orbital Hessian \mathbf{A} , along the lines of [56]

$$A'_{pq,rs} = C_{\text{HFX}} \langle \Phi_{pq\alpha\beta}^{M_S=+1} | \hat{H} | \Phi_{r\beta s\alpha}^{M_S=-1} \rangle. \quad (10.26)$$

The orbital Hessian that is used in practice is then $\mathbf{A}_k + \mathbf{A}'$, for $k = t$ or s in Eq. (10.25).

10.3.2.2 Applications

MRSF-TDDFT has several advantages over SF-TDDFT, the most significant being that spin contamination is drastically reduced, simplifying the identification of relevant states. This is important for excited-state geometry optimization, reaction-path following, and

TSH simulations. (Notably, the analytic gradient has been formulated for MRSF-TDDFT [56], along with approximate nonadiabatic couplings [55], whereas no analytic gradient for SA-SF-TDDFT is yet available.)

MECP geometries are found to be in good agreement with multireference benchmarks but also in good agreement with the simple SF-TDDFT method [57], whereas vertical excitation energies are comparable in accuracy or slightly better with MRSF [39]. Both of these comparisons are based on the BH&HLYP functional, which is also used in nearly all of the SF-TDDFT results quoted in this chapter. Interestingly, when the fraction of exact exchange (C_{HFX}) is optimized in order to minimize errors in vertical excitation energies of polyenes, the MRSF-TDDFT approach lands on $C_{\text{HFX}} = 0.5$ as the optimal value, corresponding precisely to the BH&HLYP functional. The same optimization procedure applied to LR-TDDFT lands on $C_{\text{HFX}} = 0.2$ as the optimal value, corresponding to B3LYP [40]. This observation further corroborates the idea that 50% HFX is close to optimal for collinear spin-flip methods.

TSH simulations of thymine photodynamics have been reported using MRSF-TDDFT [85], which support trapping on S_1 as the explanation for a long-lived (~ 5 ps) decay component time-resolved experiments. This is consistent with multireference results that include dynamical electron correlation [107], but it is at odds with CASSCF predictions that indicate trapping on S_2 [42]. The discrepancy appears to originate in an excited-state barrier that is too high in the absence of dynamical electron correlation, supporting other results indicating that CASSCF is not a quantitative method for excited-state dynamics [28–30].

10.4 Summary and Outlook

This chapter has surveyed systemic problems with the description of ground-state CXs in conventional LR-TDDFT. Although the focus here has been on singlet photochemistry (S_0/S_1 intersections), similar problems can be expected for any CX that involves the ground state of the molecule, when that state is used as the reference state for LR-TDDFT. Numerous (apparently successful) applications

of conventional LR-TDDFT to nonadiabatic molecular dynamics can be found in the literature, yet there are reasons to worry about that method's ability to describe the final internal conversion step that returns the molecule to its ground state. Therefore we must conclude that, at present, the situation remains unclear as to how pervasive these problems are, and the extent to which they affect real observables. There are undeniably cases where LR-TDDFT warps the topography around a S_0/S_1 intersection seam to such an extent that it has a significant effect on the simulated S_1 lifetime and thus the internal conversion timescale [134]. The unbalanced treatment of a quasi-degenerate ground and first excited state in LR-TDDFT can also lead to convergence problems that stymie attempts to use this method as a black-box engine for nonadiabatic molecular dynamics.

A "spin-flip" modification rectifies these problems, within a tractable computational formalism for which nonadiabatic (derivative) coupling vectors have been formulated and implemented based on analytic gradient theory [130, 132]. SF-TDDFT can be used in surface hopping calculations, as well as simply to locate MECPs with correct topology, including those that involve the ground state. For reasons discussed herein, SF-TDDFT calculations are typically performed using the BH&HLYP functional, and MECPs computed in this way show excellent agreement with multireference benchmarks.

A drawback of the simple SF-TDDFT approach is that it often leads to significant spin contamination in bond-breaking regions of the potential surface. For singlet photochemistry, the practical upshot is that it can be difficult to distinguish singlets from triplets in the photochemically relevant regions of the surface. State-tracking algorithms (based on wavefunction overlap) are used in practice to overcome this problem [13, 34, 133], although this feels to us like a stopgap solution. A "spin-adapted" version of the theory (SA-SF-TDDFT) has been reported [133], which solves this problem in an elegant way by introducing the minimal number of additional determinants necessary to obtain spin-pure \hat{S}^2 eigenstates, however at present its analytic gradient is not available. This method can be used to spot-check the state assignments of the simple SF-TDDFT approach. Alternatively, a "mixed reference" version of SF-

TDDFT has also been developed [54], which eliminates the spin contamination to a useful degree for low-lying singlet states, even if it does not rigorously afford spin eigenstates.

Acknowledgements

The Herbert group's work on TDDFT has been sponsored for many years by the U.S. National Science Foundation, at present under grant no. CHE-1955282.

References

1. Atchity, G. J., Xantheas, S. S., and Ruedenberg, K. (1991). Potential energy surfaces near intersections, *J. Chem. Phys.* **95**, pp. 1862–1876.
2. Barbatti, M. (2011). Nonadiabatic dynamics with trajectory surface hopping method, *WIREs Comput. Mol. Sci.* **1**, pp. 620–633.
3. Barbatti, M., and Crespo-Otero, R. (2016). Surface hopping dynamics with DFT excited states, in N. Ferré, M. Filatov, and M. Huix-Rotllant (eds.), *Density-Functional Methods for Excited States, Topics in Current Chemistry*, Vol. 368 (Springer International Publishing, Switzerland), pp. 415–444.
4. Bearpark, M. J., Robb, M. A., and Schlegel, H. B. (1994). A direct method for the location of the lowest energy point on a potential surface crossing, *Chem. Phys. Lett.* **223**, pp. 269–274.
5. Becke, A. D. (1988). Density-functional exchange-energy approximation with correct asymptotic behavior, *Phys. Rev. A* **38**, pp. 3098–3100.
6. Bernard, Y. A., Shao, Y., and Krylov, A. I. (2012). General formulation of spin-flip time-dependent density functional theory using non-collinear kernels: Theory, implementation, and benchmarks, *J. Chem. Phys.* **136**, pp. 204103:1–17.
7. Casanova, D., and Krylov, A. I. (2020). Spin-flip methods in quantum chemistry, *Phys. Chem. Chem. Phys.* **22**, pp. 4326–4342.
8. Casida, M. E. (1995). Time-dependent density functional response theory for molecules, in D. P. Chong (ed.), *Recent Advances in Density Functional Methods, Part I, Recent Advances in Computational Chemistry*, Vol. I, chap. 5 (World Scientific, River Edge, NJ), pp. 155–192.

9. Casida, M. E. (1996). Time-dependent density functional response theory of molecular systems: Theory, computational methods, and functionals, in J. M. Seminario (ed.), *Recent Developments and Applications of Modern Density Functional Theory, Theoretical and Computational Chemistry*, Vol. 4 (Elsevier, Amsterdam), pp. 391–439.
10. Casida, M. E., Gutierrez, F., Guan, J., Gadea, F.-X., Salahub, D., and Daudey, J.-P. (2000). Charge-transfer correction for improved time-dependent local density approximation excited-state potential energy curves: Analysis within the two-level model with illustration for H₂ and LiH, *J. Chem. Phys.* **114**, pp. 7062–7071.
11. Cederbaum, L. S. (2004). Born–Oppenheimer approximation and beyond, in W. Domcke, D. R. Yarkony, and H. Köppel (eds.), *Conical Intersections: Electronic Structure, Dynamics & Spectroscopy, Advanced Series in Physical Chemistry*, Vol. 15, chap. 1 (World Scientific, Singapore), pp. 3–40.
12. Chernyak, V., and Mukamel, S. (2000). Density-matrix representation of nonadiabatic couplings in time-dependent density functional (TDDFT) theories, *J. Chem. Phys.* **112**, pp. 3572–3579.
13. Closser, K. D., Gessner, O., and Head-Gordon, M. (2014). Simulations of the dissociation of small helium clusters with *ab initio* molecular dynamics in electronically excited states, *J. Chem. Phys.* **140**, pp. 134306:1–12.
14. Cordova, F., Doriol, L. J., Ipatov, A., Casida, M. E., Filippi, C., and Vela, A. (2007). Troubleshooting time-dependent density-functional theory for photochemical applications: Oxirane, *J. Chem. Phys.* **127**, pp. 164111:1–18.
15. Curchod, B. F. E., and Martínez, T. J. (2018). Ab initio nonadiabatic quantum molecular dynamics, *Chem. Rev.* **118**, pp. 3305–3336.
16. Curchod, B. F. E., Rothlisberger, U., and Tavernelli, I. (2013). Trajectory-based nonadiabatic dynamics with time-dependent density functional theory, *ChemPhysChem* **14**, pp. 1314–1340.
17. Dalgaard, E. (1982). Quadratic response functions within the time-dependent Hartree-Fock approximation, *Phys. Rev. A* **26**, pp. 42–52.
18. Dreuw, A., and Head-Gordon, M. (2005). Single-reference ab initio methods for the calculation of excited states of large molecules, *Chem. Rev.* **105**, pp. 4009–4037.
19. Elliott, P., Furche, F., and Burke, K. (2009). Excited states from time-dependent density functional theory, in K. B. Lipkowitz and T. R. Cundari (eds.), *Reviews in Computational Chemistry*, Vol. 26, chap. 3 (Wiley-VCH, New York), pp. 91–165.

20. Ernst, O. P., Lodowski, D. T., Elstner, M., Hegemann, P., Brown, L. S., and Kandori, H. (2014). Microbial and animal rhodopsins: Structures, functions, and molecular mechanisms, *Chem. Rev.* **114**, pp. 126–163.
21. Fatehi, S., Alguire, E., Shao, Y., and Subotnik, J. E. (2011). Analytic derivative couplings between configuration-interaction-singles states with built-in electron-transition factors for translational invariance, *J. Chem. Phys.* **135**, pp. 234105:1–21.
22. Fatehi, S., and Subotnik, J. E. (2012). Derivative couplings with built-in electron-transition factors: Application to benzene, *J. Phys. Chem. Lett.* **3**, pp. 2039–2043.
23. Furche, F. (2001). On the density matrix based approach to time-dependent density functional response theory, *J. Chem. Phys.* **114**, pp. 5982–5992.
24. Furche, F., and Rappoport, D. (2005). Density functional methods for excited states: Equilibrium structure and electronic spectra, in M. Olivucci (ed.), *Computational Photochemistry, Theoretical and Computational Chemistry*, Vol. 16, chap. 3 (Elsevier, Amsterdam), pp. 93–128.
25. Gao, J., Liu, W., Song, B., and Liu, C. (2004). Time-dependent four-component relativistic density functional theory for excitation energies, *J. Chem. Phys.* **121**, pp. 6658–6666.
26. Gao, J., Zou, W., Liu, W., Xiao, Y., Peng, D., Song, B., and Liu, C. (2005). Time-dependent four-component relativistic density-functional theory for excitation energies. II. The exchange-correlation kernel, *J. Chem. Phys.* **123**, pp. 054102:1–13.
27. Gherib, R., Ye, L., Ryabinkin, I. G., and Izmaylov, A. F. (2016). On the inclusion of the diagonal Born-Oppenheimer correction in surface hopping methods, *J. Chem. Phys.* **144**, pp. 154103:1–10.
28. Gozem, S., Huntress, M., Schapiro, I., Lindh, R., Granovsky, A. A., Angeli, C. and Olivucci, M. (2012). Dynamic electron correlation effects on the ground state potential energy surface of a retinal chromophore model, *J. Chem. Theory Comput.* **8**, pp. 4069–4080.
29. Gozem, S., Melaccio, F., Lindh, R., Krylov, A. I., Granovsky, A. A., Angeli, C. and Olivucci, M. (2013). Mapping the excited state potential energy surface of a retinal chromophore with multireference and equation-of-motion coupled-cluster methods, *J. Chem. Theory Comput.* **9**, pp. 4495–4506.
30. Gozem, S., Melaccio, F., Valentini, A., Filatov, M., Huix-Rotllant, M., Ferré, N., Frutos, L. M., Angeli, C., Krylov, A. I., Granovsky, A. A., Lindh,

- R., and Olivucci, M. (2014). Shape of multireference, equation-of-motion coupled-cluster, and density functional theory potential energy surfaces at a conical intersection, *J. Chem. Theory Comput.* **10**, pp. 3074–3084.
31. Grimme, S., and Waletzke, M. (1999). A combination of Kohn-Sham density functional theory and multi-reference configuration interaction methods, *J. Chem. Phys.* **111**, pp. 5645–5655.
32. Gross, E. K. U., and Kohn, W. (1990). Time-dependent density functional theory, *Adv. Quantum Chem.* **21**, pp. 255–291.
33. Gross, E. K. U., and Maitra, N. T. (2012). Introduction to TDDFT, in M. A. L. Marques, N. T. Maitra, F. M. S. Nogueira, E. K. U. Gross and A. Rubio (eds.), *Fundamentals of Time-Dependent Density Functional Theory, Lecture Notes in Physics*, Vol. 837, chap. 1 (Springer-Verlag, Heidelberg), pp. 53–97.
34. Harabuchi, Y., Keipert, K., Zahariev, F., Taketsugu, T., and Gordon, M. S. (2014). Dynamics simulations with spin-flip time-dependent density functional theory: Photoisomerization and photocyclization mechanisms of *cis*-stilbene in $\pi\pi^*$ states, *J. Phys. Chem. A* **118**, pp. 11987–11998.
35. Harabuchi, Y., Maeda, S., Taketsugu, T., Minezawa, N., and Morokuma, K. (2013). Automated search for minimum energy conical intersection geometries between the lowest two singlet states S_0/S_1 -MECIs by the spin-flip TDDFT method, *J. Chem. Theory Comput.* **9**, pp. 4116–4123.
36. Herbert, J. M., and Head-Gordon, M. (2004). Curvy-steps approach to constraint-free extended-Lagrangian *ab initio* molecular dynamics, using atom-centered basis functions: Convergence toward Born-Oppenheimer trajectories, *J. Chem. Phys.* **121**, pp. 11542–11556.
37. Herbert, J. M., Zhang, X., Morrison, A. F., and Liu, J. (2016). Beyond time-dependent density functional theory using only single excitations: Methods for computational studies of excited states in complex systems, *Acc. Chem. Res.* **49**, pp. 931–941.
38. Hirata, S., and Head-Gordon, M. (1999). Time-dependent density functional theory for radicals. An improved description of excited states with substantial double excitation character, *Chem. Phys. Lett.* **302**, pp. 375–382.
39. Horbatenko, Y., Lee, S., Filatov, M., and Choi, C. H. (2019). Performance analysis and optimization of mixed-reference spin-flip time-dependent density functional theory (MRSF-TDDFT) for vertical excitation energies and singlet-triplet energy gaps, *J. Phys. Chem. A* **123**, pp. 7991–8000.

40. Horbatenko, Y., Lee, S., Filatov, M., and Choi, C. H. (2021). How beneficial is the *explicit* account of doubly-excited configurations in linear response theory? *J. Chem. Theory Comput.* **17**, pp. 975–984.
41. Horbatenko, Y., Sadiq, S., Lee, S., Filatov, M., and Choi, C. H. (2021). Mixed-reference spin-flip time-dependent density functional theory (MRSF-TDDFT) as a simple yet accurate method for diradicals and diradicaloids, *J. Chem. Theory Comput.* **17**, pp. 848–859.
42. Hudock, H. R., Levine, B. G., Thompson, A. L., Satzger, H., Townsend, D., Gador, N., Ullrich, S., Stolow, A., and Martinez, T. J. (2007). Ab initio molecular dynamics and time-resolved photoelectron spectroscopy of electronically excited uracil and thymine, *J. Phys. Chem. A* **111**, pp. 8500–8508.
43. Huix-Rotllant, M., Natarajan, B., Ipatov, A., Wawire, C. M., Deutsch, T., and Casida, M. E. (2010). Assessment of noncollinear spin-flip Tamm-Dancoff approximation time-dependent density-functional theory for the photochemical ring-opening of oxirane, *Phys. Chem. Chem. Phys.* **12**, pp. 12811–12825.
44. Huix-Rotllant, M., Nikiforov, A., Thiel, W., and Filatov, M. (2016). Description of conical intersections with density functional methods, in N. Ferré, M. Filatov, and M. Huix-Rotllant (eds.), *Density-Functional Methods for Excited States, Topics in Current Chemistry*, Vol. 368 (Springer International Publishing), pp. 445–476.
45. Isegawa, M., and Truhlar, D. G. (2013). Valence excitation energies of alkenes, carbonyl compounds, and azabenzenes by time-dependent density functional theory: Linear response of the ground state compared to collinear and noncollinear spin-flip TDDFT with the Tamm-Dancoff approximation, *J. Chem. Phys.* **138**, pp. 134111:1–13.
46. Jain, A., Alguire, E., and Subotnik, J. E. (2016). An efficient, augmented surface hopping algorithm that includes decoherence for use in large-scale simulations, *J. Chem. Theory Comput.* **12**, pp. 5256–5268.
47. Jasper, A. W., and Truhlar, D. G. (2004). Non-Born-Oppenheimer molecular dynamics for conical intersections, avoided crossings, and weak interactions, in W. Domcke, D. R. Yarkony, and H. Köppel (eds.), *Conical Intersections: Theory, Computation and Experiment, Advanced Series in Physical Chemistry*, Vol. 17, chap. 10 (World Scientific, Singapore), pp. 375–414.
48. Keal, T. W., Koslowski, A., and Thiel, W. (2007). Comparison of algorithms for conical intersection optimisation using semiempirical methods, *Theor. Chem. Acc.* **118**, pp. 837–844.

49. Krylov, A. I. (2001). Spin-flip configuration interaction: An electronic structure model that is both variational and size-consistent, *Chem. Phys. Lett.* **350**, pp. 522–530.
50. Krylov, A. I., and Gill, P. M. W. (2013). Q-Chem: An engine for innovation, *WIREs Comput. Mol. Sci.* **3**, pp. 317–326.
51. Krylov, A. I., Sherrill, C. D., Byrd, E. F. C., and Head-Gordon, M. (1998). Size-consistent wave functions for nondynamical correlation energy: The valence active space optimized orbital coupled-cluster doubles model, *J. Chem. Phys.* **109**, pp. 10669–10678.
52. Laurent, A. D., and Jacquemin, D. (2013). TD-DFT benchmarks: A review, *Int. J. Quantum Chem.* **113**, pp. 2019–2039.
53. Lee, C., Yang, W., and Parr, R. G. (1988). Development of the Colle-Salvetti correlation-energy formula into a functional of the electron density, *Phys. Rev. B* **37**, pp. 785–789.
54. Lee, S., Filatov, M., Lee, S., and Choi, C. H. (2018). Eliminating spin-contamination of spin-flip time dependent density functional theory within linear response formalism by the use of zeroth-order mixed-reference (MR) reduced density matrix, *J. Chem. Phys.* **149**, pp. 104101:1–11.
55. Lee, S., Horbatenko, Y., Filatov, M., and Choi, C. H. (2021). Fast and accurate computation of nonadiabatic coupling matrix elements using the truncated Leibniz formula and mixed-reference spin-flip time-dependent density functional theory, *J. Phys. Chem. Lett.* **12**, pp. 4722–4728.
56. Lee, S., Kim, E. E., Nakata, H., Lee, S., and Choi, C. H. (2019). Efficient implementations of analytic energy gradient for mixed-reference spin-flip time-dependent density functional theory (MRSF-TDDFT), *J. Chem. Phys.* **150**, pp. 184111:1–11.
57. Lee, S., Shostak, S., Filatov, M., and Choi, C. H. (2019). Conical intersections in organic molecules: Benchmarking mixed-reference spin-flip time-dependent DFT (MSRF-TD-DFT) vs spin-flip TD-DFT, *J. Phys. Chem. A* **123**, pp. 6455–6462.
58. Lefrancois, D., Tuna, D., Martínez, T. J., and Dreuw, A. (2017). The spin-flip variant of the algebraic-diagrammatic construction yields the correct topology of S_1/S_0 conical intersections, *J. Chem. Theory Comput.* **13**, pp. 4436–4441.
59. Levine, B. G., Coe, J. D., and Martínez, T. J. (2008). Optimizing conical intersections without derivative coupling vectors: Application to multistate multireference second-order perturbation theory (MS-CASPT2), *J. Phys. Chem. B* **112**, pp. 405–413.

60. Levine, B. G., Ko, C., Quenneville, J., and Martínez, T. J. (2006). Conical intersections and double excitations in time-dependent density functional theory, *Mol. Phys.* **104**, pp. 1039–1051.
61. Li, X., Govind, N., Isborn, C., DePrince III, A. E., and Lopata, K. (2020). Real-time time-dependent electronic structure theory, *Chem. Rev.* **120**, pp. 9951–9993.
62. Li, Z., and Liu, W. (2010). Spin-adapted open-shell random phase approximation and time-dependent density functional theory. I. Theory, *J. Chem. Phys.* **133**, pp. 064106:1–22.
63. Li, Z., and Liu, W. (2011). Spin-adapted open-shell time-dependent density functional theory. III. An even better and simpler formulation, *J. Chem. Phys.* **135**, pp. 194106:1–14, erratum: *ibid.* **138**, 029904 (2013).
64. Li, Z., and Liu, W. (2012). Theoretical and numerical assessments of spin-flip time-dependent density functional theory, *J. Chem. Phys.* **136**, pp. 024107:1–14.
65. Li, Z., and Liu, W. (2014). First-order nonadiabatic coupling matrix elements between excited states: A Lagrangian formulation at the CIS, RPA, TD-HF, and TD-DFT levels, *J. Chem. Phys.* **141**, pp. 014110:1–10.
66. Li, Z., Liu, W., Zhang, Y., and Suo, B. (2011). Spin-adapted open-shell time-dependent density functional theory. II. Theory and pilot application, *J. Chem. Phys.* **134**, pp. 134101:1–22.
67. Li, Z., Suo, B., and Liu, W. (2014). First-order nonadiabatic coupling matrix elements between excited states: Implementation and application at the TD-DFT and pp-TDA levels, *J. Chem. Phys.* **141**, pp. 244105:1–16.
68. Liu, J., Koslowski, A., and Thiel, W. (2018). Analytic gradient and derivative couplings for the spin-flip extended configuration interaction singles method: Theory, implementation, and application to proton transfer, *J. Chem. Phys.* **148**, pp. 244108:1–11.
69. Maeda, S., Harabuchi, Y., Taketsugu, T., and Morokuma, K. (2014). Systematic exploration of minimum energy conical intersection structures near the Franck–Condon region, *J. Phys. Chem. A* **118**, pp. 12050–12058.
70. Maeda, S., Ohno, K., and Morokuma, K. (2010). Updated branching plane for finding conical intersections without coupling derivative vectors, *J. Chem. Theory Comput.* **6**, pp. 1538–1545.
71. Malhado, J. P., Bearpark, M. J., and Hynes, J. T. (2014). Non-adiabatic dynamics close to conical intersections and the surface hopping perspective, *Front. Chem.* **2**, pp. 97:1–21.

72. Marian, C. M., Heil, A., and Kleinschmidt, M. (2018). The DFT/MRCI method, *WIREs Comput. Mol. Sci.* **9**, pp. e1394:1–31, erratum: *ibid.* **9**, p. e1437 (2019).
73. Matsika, S. (2021). Electronic structure methods for the description of nonadiabatic effects and conical intersections, *Chem. Rev.* **121**, pp. 9407–9449.
74. Matsika, S., and Krause, P. (2011). Nonadiabatic events and conical intersections, *Annu. Rev. Phys. Chem.* **62**, pp. 621–643.
75. McLachlan, A., and Ball, M. (1964). Time-dependent Hartree-Fock theory for molecules, *Rev. Mod. Phys.* **36**, pp. 844–855.
76. Merer, A. J., and Mulliken, R. S. (1969). Ultraviolet spectra and excited states of ethylene and its alkyl derivatives, *Chem. Rev.* **69**, pp. 639–656.
77. Minezawa, N. (2014). Optimizing minimum free-energy crossing points in solution: Linear-response free energy/spin-flip density functional theory approach, *J. Chem. Phys.* **141**, pp. 164118:1–9.
78. Minezawa, N., and Gordon, M. S. (2011). Photoisomerization of stilbene: A spin-flip density functional theory study, *J. Phys. Chem. A* **115**, pp. 7901–7911.
79. Minezawa, N., and Nakajima, T. (2019). Trajectory surface hopping molecular dynamics simulation by spin-flip time-dependent density functional theory, *J. Chem. Phys.* **150**, pp. 204120:1–10.
80. Nelson, T. R., White, A. J., Bjorgaard, J. A., Sifain, A. E., Zhang, Y., Nebgen, B., Fernandez-Alberti, S., Mozyrsky, D., Roitberg, A. E., and Tretiak, S. (2020). Non-adiabatic excited-state molecular dynamics: Theory and applications or modeling photophysics in extended molecular materials, *Chem. Rev.* **120**, pp. 2215–2287.
81. Niehaus, T. A. (2021). Ground-to-excited derivative couplings for the density functional-based tight-binding method: Semi-local and long-range corrected formulations, *Theor. Chem. Acc.* **140**, pp. 34:1–21.
82. Ou, Q., Alguire, E. C., and Subotnik, J. E. (2015). Derivative couplings between time-dependent density functional theory excited states in the random-phase approximation based on pseudo-wavefunctions: Behavior around conical intersections, *J. Phys. Chem. B* **119**, pp. 7150–7161.
83. Ou, Q., Bellchambers, G. D., Furche, F., and Subotnik, J. E. (2015). First-order derivative couplings between excited states from adiabatic TDDFT response theory, *J. Chem. Phys.* **142**, pp. 064114:1–14.
84. Ou, Q., Fatehi, S., Alguire, E., Shao, Y., and Subotnik, J. E. (2014). Derivative couplings between TD-DFT excited states obtained by direct

- differentiation in the Tamm-Dancoff approximation, *J. Chem. Phys.* **141**, pp. 024114:1–13.
85. Park, W., Lee, S., Huix-Rotllant, M., Filatov, M., and Choi, C. H. (2021). Impact of the dynamic electron correlation on the unusually long excited-state lifetime of thymine, *J. Phys. Chem. Lett.* **12**, pp. 4339–4346.
86. Parker, S. M., Rappoport, D., and Furche, F. (2018). Quadratic response properties from TDDFT: Trials and tribulations, *J. Chem. Theory Comput.* **14**, pp. 807–819.
87. Parker, S. M., Roy, S., and Furche, F. (2016). Unphysical divergences in response theory, *J. Chem. Phys.* **145**, pp. 134105:1–12.
88. Parker, S. M., Roy, S., and Furche, F. (2019). Multistate hybrid time-dependent density functional theory with surface hopping accurately captures ultrafast thymine photodeactivation, *Phys. Chem. Chem. Phys.* **21**, pp. 18999–19010.
89. Rinkevicius, Z., Vahtras, O., and Ågren, H. (2010). Spin-flip time dependent density functional theory applied to excited states with single, double, or mixed electron excitation character, *J. Chem. Phys.* **133**, pp. 114104:1–12.
90. Rohlfing, M., and Louie, S. G. (2000). Electron-hole excitations and optical spectra from first principles, *Phys. Rev. B* **62**, pp. 4927–4944.
91. Rohrdanz, M. A., Martins, K. M., and Herbert, J. M. (2009). A long-range-corrected density functional that performs well for both ground-state properties and time-dependent density functional theory excitation energies, including charge-transfer excited states, *J. Chem. Phys.* **130**, pp. 054112:1–8.
92. Rowe, D. J. (1968). Equations-of-motion method and the extended shell model, *Rev. Mod. Phys.* **40**, pp. 153–166.
93. Rowe, D. J., and Ngo-Trong, C. (1975). Tensor equations of motion for the excitations of rotationally invariant or charge-independent systems, *Rev. Mod. Phys.* **47**, pp. 471–485.
94. Ryabinkin, I. G., Nagesh, J., and Izmaylov, A. F. (2015). Fast numerical evaluation of time-derivative nonadiabatic couplings for mixed quantum-classical methods, *J. Phys. Chem. Lett.* **6**, pp. 4200–4203.
95. Salazar, E., and Faraji, S. (2020). Theoretical study of cyclohexadiene/hexatriene photochemical interconversion using spin-flip time-dependent density functional theory, *Mol. Phys.* **118**, pp. e1764120:1–12.

96. Savin, A., Umrigar, C. J., and Gonze, X. (1998). Relationship of Kohn-Sham eigenvalues to excitation energies, *Chem. Phys. Lett.* **288**, pp. 391–395.
97. Schuurman, M. S., and Stolow, A. (2018). Dynamics at conical intersections, *Annu. Rev. Phys. Chem.* **69**, pp. 427–450.
98. Sears, J. S., Sherrill, C. D., and Krylov, A. I. (2003). A spin-complete version of the spin-flip approach to bond breaking: What is the impact of obtaining spin eigenfunctions? *J. Chem. Phys.* **118**, pp. 9084–9094.
99. Send, R., and Furche, F. (2010). First-order nonadiabatic couplings from time-dependent hybrid density functional response theory: Consistent formalism, implementation, and performance, *J. Chem. Phys.* **132**, pp. 044107:1–12.
100. Shao, Y., Head-Gordon, M., and Krylov, A. I. (2003). The spin-flip approach within time-dependent density functional theory: Theory and applications to diradicals, *J. Chem. Phys.* **118**, pp. 4807–4818.
101. Sharifzadeh, S. (2018). Many-body perturbation theory for understanding optical excitations in organic molecules and solids, *J. Phys.: Condens. Matt.* **30**, pp. 153002:1–12.
102. Sicilia, F., Blancafort, L., Bearpark, M. J., and Robb, M. A. (2008). New algorithms for optimizing and linking conical intersection points, *J. Chem. Theory Comput.* **4**, pp. 257–266.
103. Silva-Junior, M. R., Schreiber, M., Sauer, S. P. A., and Thiel, W. (2008). Benchmarks for electronically excited states: Time-dependent density functional theory and density functional theory based multireference configuration interaction, *J. Chem. Phys.* **129**, pp. 104103:1–14.
104. Small, D. W., Sundstrom, E. J., and Head-Gordon, M. (2015). A simple way to test for collinearity in spin symmetry broken wave functions: General theory and application to generalized Hartree Fock, *J. Chem. Phys.* **142**, pp. 094112:1–9.
105. Stratmann, R. E., Scuseria, G. E., and Frisch, M. J. (1998). An efficient implementation of time-dependent density-functional theory for the calculation of excitation energies of large molecules, *J. Chem. Phys.* **109**, pp. 8218–8224.
106. Subotnik, J. E., Jain, A., Landry, B., Petit, A., Ouyang, W., and Bellonzi, N. (2016). Understanding the surface hopping view of electronic transitions and decoherence, *Annu. Rev. Phys. Chem.* **67**, pp. 387–417.
107. Szymczak, J. J., Barbatti, M., Hoo, J. T. S., Adkins, J. A., Windus, T. L., Nachtigallová, D., and Lischka, H. (2009). Photodynamics simulations

- of thymine: Relaxation into the first excited singlet state, *J. Phys. Chem. A* **113**, pp. 12686–12693.
108. Tapavicza, E., Bellchambers, G. D., Vincent, J. C., and Furche, F. (2013). *Ab initio* non-adiabatic molecular dynamics, *Phys. Chem. Chem. Phys.* **15**, pp. 18336–18348.
109. Tapavicza, E., Tavernelli, I., and Rothlisberger, U. (2007). Trajectory surface hopping within linear response time-dependent density functional theory, *Phys. Rev. Lett.* **98**, pp. 023001:1–4.
110. Tavernelli, I., Röhrig, U. F., and Rothlisberger, U. (2005). Molecular dynamics in electronically excited states using time-dependent density functional theory, *Mol. Phys.* **103**, pp. 963–981.
111. Tavernelli, I., Tapavicza, E., and Rothlisberger, U. (2009). Non-adiabatic dynamics using time-dependent density functional theory: Assessing the coupling strengths, *J. Mol. Struct. (Theochem)* **914**, pp. 22–29.
112. Tavernelli, I., Tapavicza, E., and Rothlisberger, U. (2009). Nonadiabatic coupling vectors within linear response time-dependent density functional theory, *J. Chem. Phys.* **130**, pp. 124107:1–10.
113. Tretiak, S., and Mukamel, S. (2002). Density matrix analysis and simulation of electronic excitations in conjugated and aggregated molecules, *Chem. Rev.* **102**, pp. 3171–3212.
114. Tully, J. C. (1990). Molecular dynamics with electronic transitions, *J. Chem. Phys.* **93**, pp. 1061–1071.
115. Uratani, H., Morioka, T., Yoshikawa, T., and Nakai, H. (2020). Fast nonadiabatic molecular dynamics via spin-flip time-dependent density-functional tight-binding approach: Application to nonradiative relaxation of tetraphenylethylene with locked aromatic rings, *J. Chem. Theory Comput.* **16**, pp. 7299–7313.
116. Uratani, H., Yoshikawa, T., and Nakai, H. (2021). Trajectory surface hopping approach to condensed-phase nonradiative relaxation dynamics using divide-and-conquer spin-flip time-dependent density-functional tight binding, *J. Chem. Theory Comput.* **17**, pp. 1290–1300.
117. Wand, A., Gdor, I., Zhu, J., Sheves, M., and Ruhman, S. (2013). Shedding new light on retinal protein photochemistry, *Annu. Rev. Phys. Chem.* **64**, pp. 437–458.
118. Wang, F., and Liu, W. (2003). Comparison of different polarization schemes in open-shell relativistic density functional calculations, *J. Chin. Chem. Soc. (Taipei)* **50**, pp. 597–606.

119. Wang, F., and Ziegler, T. (2004). Time-dependent density functional theory based on a noncollinear formulation of the exchange-correlation potential, *J. Chem. Phys.* **121**, pp. 12191:1–6.
120. Wang, F., and Ziegler, T. (2005). The performance of time-dependent density functional theory based on a noncollinear exchange-correlation potential in the calculations of excitation energies, *J. Chem. Phys.* **122**, pp. 074109:1–9.
121. Wang, L., Akimov, A., and Prezhdo, O. V. (2016). Recent progress in surface hopping: 2011–2015, *J. Phys. Chem. Lett.* **7**, pp. 2100–2112.
122. Wang, L., Qiu, J., Bai, X., and Xu, J. (2020). Surface hopping methods for nonadiabatic dynamics in extended systems, *WIREs Comput. Mol. Sci.* **10**, pp. e1435:1–24.
123. Weiss, H., Ahlrichs, R., and Häser, M. (1993). A direct algorithm for self-consistent-field linear response theory and application to C₆₀: Excitation energies, oscillator strengths, and frequency-dependent polarizabilities, *J. Chem. Phys.* **99**, pp. 1262–1270.
124. Xu, X., Yang, K. R., and Truhlar, D. G. (2014). Testing noncollinear spin-flip, collinear spin-flip, and conventional time-dependent density functional theory for predicting electronic excitation energies of closed-shell atoms, *J. Chem. Theory Comput.* **10**, pp. 2070–2084.
125. Yarkony, D. R. (2001). Nuclear dynamics near conical intersections in the adiabatic representation: I. The effects of local topography on interstate transitions, *J. Chem. Phys.* **114**, pp. 2601–2613.
126. Yu, L., Xu, C., Lei, Y., Zhu, C., and Wen, Z. (2014). Trajectory-based nonadiabatic molecular dynamics without calculating nonadiabatic coupling in the avoided crossing case: *Trans* ↔ *cis* photoisomerization in azobenzene, *Phys. Chem. Chem. Phys.* **16**, pp. 25883–25895.
127. Yue, L., Lan, Z., and Liu, Y.-J. (2014). The theoretical estimation of the bioluminescent efficiency of the firefly via a nonadiabatic molecular dynamics simulation, *J. Phys. Chem. Lett.* **6**, pp. 540–548.
128. Yue, L., Liu, Y., and Zhu, C. (2018). Performance of TDDFT with and without spin-flip in trajectory surface hopping dynamics: *Cis-trans* azobenzene photoisomerization, *Phys. Chem. Chem. Phys.* **20**, pp. 24123–24139.
129. Yue, L., Yu, L., Xu, C., Lei, Y., Liu, Y., and Zhu, C. (2017). Benchmark performance of global switching versus local switching for trajectory surface hopping molecular dynamics simulation: *Cis* ↔ *trans* azobenzene photoisomerization, *Chem. Phys. Chem.* **18**, pp. 1274–1287.

130. Zhang, X., and Herbert, J. M. (2014). Analytic derivative couplings for spin-flip configuration interaction singles and spin-flip time-dependent density functional theory, *J. Chem. Phys.* **141**, pp. 064104:1–9.
131. Zhang, X., and Herbert, J. M. (2014). Excited-state relaxation pathways in uracil versus hydrated uracil: Solvatochromatic shift in the $^1n\pi^*$ state is the key, *J. Phys. Chem. B* **118**, pp. 7806–7817.
132. Zhang, X., and Herbert, J. M. (2015). Analytic derivative couplings in time-dependent density functional theory: Quadratic response theory versus pseudo-wavefunction approach, *J. Chem. Phys.* **142**, pp. 064109:1–12.
133. Zhang, X., and Herbert, J. M. (2015). Spin-flip, tensor equation-of-motion configuration interaction with a density-functional correction: A spin-complete method for exploring excited-state potential energy surfaces, *J. Chem. Phys.* **143**, pp. 234107:1–10.
134. Zhang, X., and Herbert, J. M. (2021). Nonadiabatic dynamics with spin-flip versus linear-response time-dependent density functional theory: A case study for the protonated Schiff base $C_5H_6NH_2^+$, *J. Chem. Phys.* **155**, pp. 124111:1–15.